

# Elastic scattering at $\sqrt{s} = 6$ GeV up to $\sqrt{s} = 13$ TeV (proton-proton; proton-antiproton; proton-neutron)

O.V. Selyugin

*BLTP, Joint Institute for Nuclear Research, 141980 Dubna, Moscow region, Russia*

In the framework of the Regge-eikonal model of hadron interaction based on the analyticity of the scattering amplitude with taking into account the hadron structure, a simultaneous analysis is carried out of 90 sets of data. These sets include the data were obtained at low energies ( $\sqrt{s} > 3.6$  GeV and high energies at FNAL, ISR,  $SP\bar{P}S$ , TEVATRON and LHC with 4326 experimental points, including the polarization data of analysing power. The energy and momentum transfer dependence of separate sets of data is analyzed on the basis of the eikonized Born amplitude with taking into account two additional anomalous terms. Different origins of the nonlinear behavior of the slope of the scattering amplitude are compared. No contribution of hard-Pomeron in the elastic hadron scattering is found. The importance of Odderon's contribution is presented. The form and energy dependence of different terms of the cross-even and cross-odd parts of the elastic nucleon-nucleon scattering amplitude is determined in the framework of the High Energy Generalize Structure (HEGS) model. In the framework of the HEGS model, using the electromagnetic and gravitomagnetic form factors, the differential cross sections in the Coulomb Nuclear Interference (CNI) region and at large momentum transfer are described well in a wide energy region simultaneously. It is shown that the cross-even part includes the soft pomeron and the additional term with a large slope have energy dependence  $\ln^2(s)$ . The cross-odd part includes the maximal odderon term with  $\ln^2(s)$  and an additional oscillation term with  $\ln(s)$ . It is shown that the additional terms with large slope are proportional to charge distributions but the maximal odderon term and oscillation term are proportional to matter distributions. Also, a good description of proton-neutron differential scattering with 526 experimental points is obtained on the basis of the amplitudes taken from the analysis of  $pp$  and  $p\bar{p}$  scattering. A good enough description of the polarization data was also obtained.

PACS numbers: 11.80.Cr, 12.40.Nn, 13.85.Dz

## I. INTRODUCTION

One of the most important tasks of modern physics is the research into the basic properties of hadron interactions. The dynamics of strong interactions finds its most complete representation in elastic scattering. It is just this process that allows the verification of the results obtained from the main principles of quantum field theory: the concept of the scattering amplitude as a unified analytic function of its kinematic variables connecting different reaction channels was introduced in the dispersion theory by N.N. Bogoliubov[1]. Now many questions of hadron interactions are connected with modern problems of astrophysics such as unitarity and the optical theorem [2], and problems of baryon-antibaryon symmetry and CP-invariance violation [3]. Many models predict that soft hadron interactions will enter a new regime at the LHC: given the huge energy, the S-matrix reaches the unitarity limit. The main domain of elastic scattering is small angles. Only in this region of interactions we can measure the basic properties that define the hadron structure. Their values are connected, on the one hand, with the large-scale structure of hadrons and, on the other hand, with the first principles that lead to theorems on the behavior of scattering amplitudes at asymptotic energies [4, 5].

The research of the structure of the elastic hadron scattering amplitude at superhigh energies and small mo-

mentum transfer -  $t$  can give a connection between the experimental knowledge and the basic asymptotic theorems based on first principles [5–7]. This gives information about the hadron interaction at large distances where the perturbative QCD does not work [8, 9, 11] and a new theory as, for example, instanton or string theories must be developed.

The structure of hadrons reflected in generalized parton distributions (GPDs) is now one of the most interesting questions of the physics of strong interactions (see, for example, [12, 13]. This is tightly connected with the spin physics of the hadron [14]. Some modern accelerator experiments have developed extensive programs for deep studies of different issues related to this problem. For example, the Jefferson Laboratory/Electron-Ion Collider (EIC) team intends to extract generalized parton distributions (GPDs) [15]. The same problem is posed for future experiments at the SPD of NICA-JINR [16].

Recent studies of elastic scattering of high energy protons lead to several unexpected results reviewed, e.g., in [9, 10]. Spin amplitudes of the elastic  $NN$  scattering constitute a spin picture of the nucleon. Without knowing of the spin  $NN$ -amplitudes, it is impossible to understand the spin observable of nucleon scattering off nuclei. In the modern picture, the structure of hadrons is determined by GPDs which include the corresponding parton distributions (PDFs). The sum rules [17–20] allow one to obtain the elastic form factor (electromagnetic and gravitomagnetic) through the first and second integration

moments of GPDs [21]. This leads to remarkable properties of GPDs, some corresponding to inelastic and elastic scattering of hadrons. Now different models examining the nonperturbative instanton contribution lead to sufficiently large spin effects at superhigh energies [22–25]. The research of such spin effects will be a crucial stone for different models and will help us to understand the interaction and structure of particles, especially at large distances. There are large programs of researching spin effects at different accelerators. Especially, we should like to note the programs at the NICA where the polarization of both the collider beams will be constructed. So it is very important to obtain reliable predictions for spin asymmetries at these energies. In this paper, we extend the model predictions to spin asymmetries in the NICA energy domain.

The unique experiment carried out by the TOTEM Collaboration at the LHC at 13 TeV gave excellent experimental data on the elastic proton-proton scattering in a wide region of transfer momenta [26, 27]. It is especially necessary to note the experimental data obtained at a small momentum transfer in the Coulomb-hadron interference region. The experiment reaches very small  $t = 8 \cdot 10^{-4} \text{ GeV}^2$  with small  $\Delta t$ , which give a large number of experimental points in a sufficiently small region of momentum transfer. This allows one to carry out careful analysis of the experimental data to explore some properties of hadron elastic scattering.

There are two sets of data - at a small momentum transfer [26] and at a middle and large momentum transfer [27]. They overlap in some region of the momentum transfer, which supplies practically the same normalization of both sets of differential cross sections of elastic proton-proton scattering. Recently, the first set of data has created a wide discussion of the determination of the total cross section and the value of  $\rho(t=0)$  [28].

There is a very important characteristic of the elastic scattering amplitude such as the ratio of the real part to imaginary part of the scattering amplitude -  $\rho(s,t)$ . It is tightly connected with the integral and differential dispersion relations. Of course, especially after different results obtained by the UA4 and UA4/2 Collaborations, physicists understand that  $\rho(s,t=0)$  is not a simple experimental value but heavily depends on theoretical assumptions about the momentum dependence of the elastic scattering amplitude. Our analysis of both experimental data obtained by the UA4 and UA4/2 Collaborations shows a small difference value of  $\rho(s,t=0)$  obtained in both the experiments if the nonlinear behaviour of the elastic scattering amplitude is taken into account [29]. Hence, this is not an experimental problem but a theoretical one [30].

For extraction of the sizes of  $\sigma_{tot}$  and  $\rho(t=0)$  the Coulomb hadron region of momentum transfer is used (for example [26]). However, the form of the scattering amplitude assumed for small  $t$  and satisfying the existing experimental data at small momentum transfer can essentially be different from experimental data at large  $t$ .

One should take into account the analysis of the differential cross section at 13 TeV where the diffraction minimum impacts the form of  $d\sigma/dt$  already at  $t = -0.45 \text{ GeV}^2$ .

The analysis of new effects discovered on the basis of the experimental data at 13 TeV [30–32] and associated with the specific properties of the hadron potential at large distances was carried out with taking account all sets of experimental data on elastic  $pp$ -scattering obtained by the TOTEM and ATLAS Collaborations in a wide momentum transfer region and gave a quantitative description of all examined experimental data with minimum fitting parameters.

The non-linear behavior of the slope of the differential cross sections at a small momentum transfer, which was announced by the TOTEM Collaboration in the proton-proton elastic scattering at 8 TeV, shows that the complex (complicated) form of strong interactions searched out at low energies remains at superhigh energies too. This means that the strong interaction is not simplified at superhigh energies but includes many different parts of the hadron potential.

Using the existing model of nucleon elastic scattering at high energies  $\sqrt{s} = [3.6 - 14] \text{ TeV}$  [33, 34], which involves minimum of free parameters, we are going to develop its extended version aimed to describe all available data on cross sections and spin-correlation parameters at lower energies down to the SPD NICA region. The model will be based on the usage of known information on GPDs in the nucleon, electro-magnetic and gravitomagnetic form factors of the nucleon taking into account analyticity and unitarity requirements and providing compatibility with the high energy limit, where the pomeron exchange dominates.

The structure of the paper is as follows: in Section 2 the basic picture of diffraction scattering is discussed including the nonlinear behavior of the slope of the differential cross section at small momentum transfer. In Section 3 the experimental data base used in the analysis is reviewed. In section 4 the asymptotic structure of the scattering amplitude is discussed shortly and the form factors used are particularly considered. Section 5 presents the different model approximations used in the model and the structure of the scattering amplitude. In section 6 the results of the fitting procedure and the behavior of the imaginary and real parts of the elastic scattering amplitude are considered. In section 7 the impact of the value of  $\rho(s,t)$  and odderon contributions on the differential cross sections is analysed. Section 8 discusses new effects discovered during the model analysis of experimental data. In section 9 the obtained results for proton-neutron elastic scattering are presented. In section 10 the results of the model calculations of the spin correlation parameter  $A_N(s,t)$  are present. Finally, the obtained results and some predictions of our model are discussed in Section 11.

## II. SMALL MOMENTUM TRANSFER REGION

### A. Electromagnetic scattering

The  $t$  dependence of the elastic peak is one of the important issues, which can also be related to optics. At high energy, elastic scattering at small angles has some similarity with light scattering in the Fresnel region. The amplitude for the electric field propagating in the  $z$  direction is given by the Rayleigh-Sommerfeld equation

$$E(x, y, z) = -\frac{i}{\lambda} \int \int_{-\infty}^{+\infty} E(x', y', 0) \frac{e^{ikr}}{r} \cos \theta dx' dy' \quad (1)$$

where  $r = \sqrt{(x-x')^2 + (y-y')^2 + z^2}$ , and  $\cos \theta = \frac{z}{r}$ . The integral can be performed analytically only for the simplest geometrical cases. At  $x = kR \gg 1$  it can be obtained [35]

$$\mathcal{A}(\theta) \propto \frac{iJ_1(x \sin \theta)}{\sin \theta}$$

Hence, even in the simplest case the elastic peak cannot be described by a simple exponential. Note that this form of the scattering amplitude is used in diffractive hadron scattering.

### B. Hadron scattering

In ref. [36], the TOTEM Collaboration announced the observation of the non-exponential behavior of the differential elastic cross sections at 8 TeV and small momentum transfer  $|t|$ . Of course, the form of the elastic peak depends also on the structure of particles and the dynamics of the interaction. These two features can be parameterised by the profile function  $\rho(\vec{b})$  (in the space of impact parameter,  $\vec{b}$ ) or by the elastic form factor (in momentum space). For example, in [37] different forms of the profile function determined by the density distributions taking part in the interaction were considered:

$$\begin{aligned} \text{circle of radius } b_0 = 4 \text{ GeV}^{-1} \\ \Rightarrow \mathcal{A}(t) \propto J_0(4\sqrt{|t|}); \end{aligned} \quad (2)$$

$$\begin{aligned} \text{hollow disk near } b_0 = 2.8 \text{ GeV}^{-1} \\ \Rightarrow \mathcal{A}(t) \propto e^{2.8t} J_0(2.8\sqrt{|t|}); \end{aligned} \quad (3)$$

$$\begin{aligned} \text{black disk of radius } 6 \text{ GeV}^{-1} \\ \Rightarrow \mathcal{A}(t) \propto J_1(6\sqrt{|t|})/(6\sqrt{|t|}); \end{aligned} \quad (4)$$

$$\rho(b) \sim e^{-cb} \Rightarrow \mathcal{A}(t) \propto e^{5t}; \quad (5)$$

$$\rho(b) \sim e^{\mu\sqrt{b_0^2+b}} \Rightarrow \mathcal{A}(t) \propto e^{5(\sqrt{4\mu^2-t}-2\mu)}. \quad (6)$$

The  $t$  dependence of these amplitudes is shown in Fig. 1. Clearly, the simple exponential form (5) is a special separate case. We can see, except for the last case (eq.6), that if we take a small interval of  $t$  (for example,  $0.01 < |t| < 0.15 \text{ GeV}^2$ ) the curves give practically the same

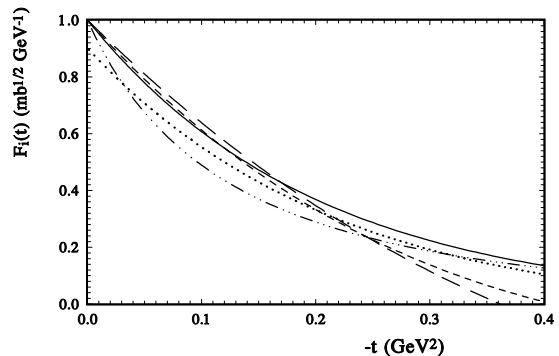


FIG. 1. Possible  $t$  dependences of the scattering amplitude  $\mathcal{A}(t)$ , rescaled to unity at  $t = 0$ . (solid line - for Eq. (5); long-dashed line - for Eq. (2); short-dashed line - for Eq. (4); dotted line - for Eq. (3), and dashed-dotted line - for Eq. (6).

result, especially the lines of eqs. 3,5,6. However, they give essentially different results on some larger values of  $t$  or as  $t \rightarrow 0$ . Hence, to obtain the true form of the scattering amplitude, it is necessary to take experimental data in a wider interval of  $t$  and tending to the limit  $t \rightarrow 0$ .

This simplest approximation of the differential cross section by one exponent with a constant slope can lead to artificial new effects. For example, in the experiment at the Protvino accelerator on elastic proton-proton scattering there were found "oscillations" at a small momentum transfer [38]. However, in [39] it was shown that such "oscillations" can appear when the differential cross section is described by two exponentials with different slopes and one exponential with the constant slope.

The investigation of the energy and  $t$  dependence of the slope of the elastic peak can lead to new information about the structure of interacting particles. Early measurements at ISR revealed four slopes of differential cross section in different regions of momentum transfer, which result from the complicated structure of nucleons.

### C. Non-linear slope

The complicated  $t$  dependence of the slope can have many origins. First of all, it comes from the unitarization procedure of the Born term of the elastic scattering amplitude. In many purely phenomenological analyses it is represented by the  $Ct^2$  term in the slope that mimics the unitarization procedure. The hadron structure is reflected also not only at a large momentum transfer but also at small  $t$ . This especially concerns the meson clouds whose interaction in many models is added to the central part of hadrons (for example, in the Pomplin model [40] and the Dubna Dynamical (DD) model [41] which leads

to the  $\sqrt{t_0 + t}$  dependence of the scattering amplitude). Such a complicated hadron structure can be reflected in the presence of two form factors - electromagnetic and mater form factor of hadrons (for example, the HEGS model [33, 34]).

Another term of the slope, which is commonly represented as

$$\sqrt{4\mu^2 - t} - 2\mu, \quad (7)$$

is used in many phenomenological descriptions of the elastic differential cross sections to explain the "break" in the differential cross sections. Note that an additional term in the slope like  $\sqrt{t_0 - t}$  was obtained earlier whose first approximation can be related to absorbtion corrections that can produce a set of canceling Regge cuts [42, 43] and leads to the Schwarz type trajectories [44]  $\alpha(t) = 1 + \gamma t^{1/2}$ . A more complicated form was obtained in [45]  $\alpha_{\pm}(t) = 1 \pm \gamma t^{1/2} + 2\rho(1/2 \gamma^2 t)^{3/2}(-\ln(t))^{1/2}$ . The appearance of a complex trajectory greatly complicates the picture and requires additional research. Hence, in [46], based on the works [47, 48], it was proposed to use the simplest form  $\alpha(t) = 1.041 - 0.15\sqrt{t_0 - t}$ . However, as we show, such behavior has a really pure phenomenological basis and can be replaced by either a simpler form (for example, eq.(7) or a more complicated form used in the HEGS-model [34]).

Many models based on the famous works [49, 50] researched the non-linear behavior of the scattering amplitude. Based on the works in [51], it was obtained that

$$\alpha_P(q^2) = 1 - C_p q^2 - (\sigma_{\pi\pi}/32\pi^2)h_1(q^2). \quad (8)$$

where

$$h_1(q^2) = \frac{q^2}{\pi} \left[ \frac{8\mu^2}{q^2} - \left( \frac{4\mu^2 + q^2}{q^2} \right)^{3/2} \ln \frac{\sqrt{4\mu^2 + q^2} + q}{\sqrt{4\mu^2 + q^2} - q} + \ln \frac{m^2}{\mu^2} \right], \quad (9)$$

with  $q^2 = -t$ . Note that we have removed the misprint in this equation, as made in [52, 53]. They obtained the limits of the representation in the brackets at  $q^2 \gg 4\mu^2$ ; hence, the slope grows in order  $q^2$  with small logarithmic suppression. At small  $t$  ( $q^2 \ll 4\mu^2$ ) they predicted that the representation in the brackets goes to  $\ln(m^2/\mu^2) - 8/3$ . Note that the authors aimed to explain the deviation of the slope from the constant at a non-small momentum transfer (in the domain  $-t = 0.4 \text{ GeV}^2$ ). However, in this domain the impact of the diffraction minimum is already felt. Hence this domain of  $t$  is usually described by an additional term like  $ct^2$ , which were proposed earlier (for example [54]).

Practically at the same time a similar equation was obtained in [55]

$$D_R^{NN}(t) = n \left[ A - \left( \frac{(4\mu^2 + q^2)^{3/2}}{q} \right) \ln \frac{\sqrt{4\mu^2 + q^2} + q}{\sqrt{4\mu^2 + q^2} - q} \right]^{-1} \quad (10)$$

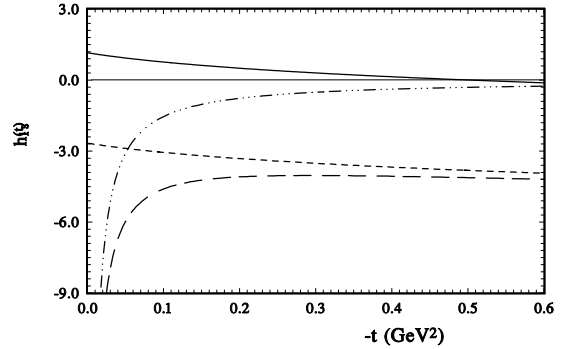


FIG. 2. The  $t$  dependence of the different parts of the terms of eq.(9) (solid line - the sum of all three terms in the brackets; the dots-dashed line - the first term is multiplied by  $(-1)$ ; the long-dashed line - the second term, the short-dashed line - the sum of the two first terms).

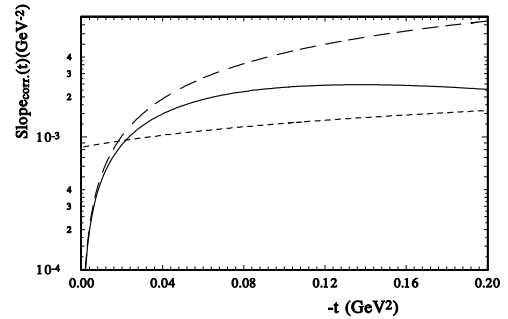


FIG. 3. The  $t$  dependence of the additional terms to  $\alpha't$  (solid line - eq.(9); long-dashed line - eq.(7); short-dashed line - eq.(7) without extraction of  $2\mu$  and multiplied by 0.1).

They proposed to approximate this representation by

$$D_R^{NN}(t) \sim \left[ \frac{1}{5\mu^2 - t} + C_{const} \right] \quad (11)$$

For numerical calculation and comparison with experimental data, they took  $C_{const} = 24.3 \text{ GeV}^{-2}$ .

In [52], using the calculations [51] and removing the misprint, the authors proposed for  $h_1$ , with taking into account the meson form factor (with  $\Lambda_\pi^2 = m_\rho^2 \text{ GeV}^2$ ), the following equation:

$$h_1(q^2) = \frac{4}{\tau} f_\pi^2(t) [2\tau - (1 + \tau)^{3/2}] \ln \frac{\sqrt{1 + \tau} + 1}{\sqrt{1 + \tau} - 1} + \ln \frac{m^2}{\mu^2}, \quad (12)$$

where  $\tau = 4\mu^2/q^2$  and

$$f_\pi(t) = \frac{\Lambda_\pi^2}{\Lambda_\pi^2 - t} \quad (13)$$

Really, for the slope, which is multiplied by  $q^2$ , there are two divergence terms with different signs plus a small constant term. The divergence terms cancel each other and the rest have a slow  $t$  dependence (see Fig. 2). The cancelation of the two terms as  $t \rightarrow 0$  is not full and the rest have also some indefiniteness and strongly depend on  $t$ . In Fig. 2, the  $t$  dependence of the different parts of the term of eq.(9) in the brackets is shown. The cancelation of the two diverse terms leads to the negative contribution to the standard constant slope. However, the sum of all three terms gives a positive additional contribution with a small  $t$  dependence.

In Fig. 3, we show the  $t$  dependence of a different form of the slopes with the full kinematic coefficient. One can see a very different  $t$  dependence, especially in the form  $\sqrt{4\mu^2 + q^2}$  which was proposed in [46] without the extraction of  $2\mu$ . Some models of hadron interactions at high energy suppose that the slope has a slow  $t$  dependence. For example, the Dubna dynamical model (DDm) [41], which takes into account the contribution to hadron interactions from the meson cloud of the nucleon and uses the standard eikonal form of the unitarization, leads to the scattering amplitude in the form

$$T(s, t) = -is \sum_{n=1}^{\infty} \frac{\mu}{(n^2\mu^2 - t)^{3/2}} \quad (14)$$

$$(1 - b\sqrt{n^2\mu^2 - t})e^{-b\sqrt{n^2\mu^2 - t}}.$$

The analysis of the high energy data on the proton-antiproton scattering in the framework of this model shows the obvious non-exponential behavior of the differential cross sections. For  $\sqrt{s} = 540$  GeV it shows the change in the slope from  $16.8 \text{ GeV}^{-2}$  at  $t = -0.001 \text{ GeV}^2$  up to  $14.9 \text{ GeV}^{-2}$  at  $t = -0.12 \text{ GeV}^2$ . For the same  $t$  the size of  $\rho(s, t)$  changes from 0.141 up to 0.089. For Tevatron energy  $\sqrt{s} = 1800$  GeV it shows the change of the slope from  $18.1 \text{ GeV}^{-2}$  at  $t = -0.001 \text{ GeV}^2$  up to  $15.9 \text{ GeV}^{-2}$  at  $t = -0.12 \text{ GeV}^2$  and again the size of  $\rho(s, t)$  changes from 0.182 up to 0.143. Hence, the model shows the continuously decreasing slope and  $\rho$  at small  $t$ . Practically the same results were obtained in [40] in the framework of the model that also uses the eikonal unitarization.

The analysis [29] of the high precision data obtained at *SPPS* at  $\sqrt{s} = 541$  GeV in the UA4/2 experiment shows the existence in the slope of the term proportional to  $\sqrt{|t|}$ . This term can be related with the nearest  $\pi$  meson threshold or, as was shown in [29], such behavior of the differential cross sections can reflect the presence of the contribution of the spin-flip amplitude. As was noted in [56]), the analytic  $S$ -matrix theory, perturbative quantum chromodynamics and the data require Regge trajectories to be nonlinear complex functions [57, 58]. The

Pomeron trajectory has threshold singularities, the lowest one being due to the two-pion exchange required by the  $t$ -channel unitarity [51]. This threshold singularity appears in different forms in various models (see [56]). In the recent high energy general structure model (HEGS) [34], a small additional term is introduced into the slope which reflects some possible small nonlinear properties of the intercept. As a result, the slope is taken in the form

$$B(s, t) = -\alpha' \ln(\hat{s})[1 - d_1 t / \ln(\hat{s}) e^{d_2 \alpha_1 t \ln(\hat{s})}]. \quad (15)$$

This form leads to the standard form of the slope as  $t \rightarrow 0$  and  $t \rightarrow \infty$ . Note that our additional term at large energies has a similar form as the additional term to the slope coming from  $\pi$ -loop examined in [51] and recently in [52].

### III. EXPERIMENTAL DATABASE

In our research, we use the widest region of experimental data. The energy region begins from  $\sqrt{s} = 3.5 - 3.8$  GeV for proton-antiproton scattering. At these energies new data were obtained in the high precision experiment on elastic  $p\bar{p}$  scattering at small angles. It has four sets at different energies in the momentum transfer region  $|t| = [0.000986 - 0.02] \text{ GeV}^2$  [59]. This experiment is very important as they obtained the value of  $\rho(s, t = 0)$  with a remarkably small error and with the size near zero. It is essentially different from the value of  $\rho(s, t = 0)$  obtained in the framework of the dispersion relation analysis by P. Kroll, which was carried out on the basis of old experimental data with large errors.

Low-energy proton-antiproton data from  $\sqrt{s} = 11.54$  GeV up to the final ISR energy  $\sqrt{s} = 62$  GeV are represented in eleven sets [61]. Then we include seven sets of experimental data obtained at the *SPPS* collider at energies around  $\sqrt{s} = 540 - 630$  GeV. The Tevatron data at  $\sqrt{s} = 1800 - 1960$  GeV are represented in four sets. The latter data present the maximal energy obtained for the proton-antiproton scattering at accelerators. On the whole, for the  $p\bar{p}$  elastic scattering we have 33 sets of the different experiments.

For the proton-proton elastic scattering we take into account sixty five sets of different experiments from the low energy  $\sqrt{s} = 6.1$  GeV up to the maximal LHC energy  $\sqrt{s} = 13$  TeV [62, 63]. We especially note the high precision experimental data obtained at a small momentum transfer by the FNAL collaborations at  $\sqrt{s} = 9.8, 9.9, 10.6, 12.3$  GeV and at  $\sqrt{s} = 19.4, 22.2, 23.9, 27.4$  GeV which start from a very small momentum transfer  $t = -0.00049 \text{ GeV}^2$ . They can be compared with the data obtained by the UA4/2 Collaboration at the *SPPS* collider, which start from  $t = -0.000875 \text{ GeV}^2$  and with the data obtained at the LHC by the TOTEM Collaboration at  $\sqrt{s} = 13$  TeV which reached the  $t = -0.00029 \text{ GeV}^2$ . Of course, the last case achieved the smallest possible angles of scattering. We take into account the experimental data at a high value of momentum transfer

up to momentum transfer  $-t = 10 - 14 \text{ GeV}^2$ . The corresponding experimental data were obtained at energies  $\sqrt{s} = 19.4, 27.4, 52.8 \text{ GeV}$ .

Summarizing all the sets of experimental data on elastic scattering at not large angles, we took into account 115 sets of different experiments which included 4326 experimental points on proton-proton and proton-antiproton elastic scattering.

We included in our simultaneous analysis the data for the spin correlation parameter  $A_N(s, t)$  of the polarized proton-proton elastic scattering. This set of data includes 235 experimental data for relatively small energies  $\sqrt{s} = 3.63 \text{ GeV}$  and up to  $\sqrt{s} = 23.4 \text{ GeV}$ . During our fitting procedure sufficiently good descriptions of the experimental data were obtained.

For the first time, we also included in our research the elastic proton-neutron experimental data. The corresponding data were taken into account beginning from the  $\sqrt{s} = 4.5 \text{ GeV}$  up to maximal energy proton-neutron collisions  $\sqrt{s} = 27.19 \text{ GeV}$  obtained at accelerators. It should be noted that such energy represented an average between minimum and maximum energies. For example, maximum energy obtained at the FNAL presented average between  $P_L = 340 \text{ GeV}/c$  and  $P_L = 400 \text{ GeV}/c$ . It is very important that in such experiments a very small momentum transfer was reached, for example  $-t_{min} = 0.23 \cdot 10^{-4} \text{ GeV}^2$  at  $\sqrt{s} = 23.193 \text{ GeV}$ . On the whole, we took into account 24 sets of experimental data of different experiments which supply 526 experimental data. Hence, on the whole, we took into our analysis 5027 experimental data on elastic nucleon-nucleon scattering.

#### IV. MAIN AMPLITUDES OF THE HIGH ENERGY GENERALIZED STRUCTURE (HEGS) MODEL

##### A. Asymptotic part of the scattering amplitude

The model is based on the idea that at high energies a hadron interaction in the non-perturbative regime is determined by the non-perturbative Regge gluons exchange. The cross-even part of this amplitude can have two non-perturbative parts, possible standard non-perturbative QCD pomeron - ( $P_{2np}$ ) and cross-even part of 3-non-perturbative gluons ( $P_{3np}$ ). The interaction of these two objects is proportional to two different form factors of the hadron and both form factors are discussed in the next subsection. This is the main assumption of the model. Both terms have the same intercept. This corresponds to the maximal Odderon, which was introduced by L. Lukaszuk, B. Nicolescu [64].

Note, the Odderon that arises naturally in perturbative QCD, for example [65], with the intercept  $\alpha_{Odd}(0) = 1$ . They show that shadowing corrections decreased Odderon contributions. However, the experimental data show the Odderon contribution at ISR energy  $\sqrt{s} = 52.8 \text{ GeV}$  and at Tevatron energy [66] and probably at LHC energy

$\sqrt{s} = 13 \text{ TeV}$ . For example, in [67] it was noted "On the other hand, it is possible to introduce the Odderon phenomenologically as an object which does not violate first principles and the axiomatic theorems. In fact it was stated in [28] that the new TOTEM result is a definitive confirmation of the experimental discovery of the Odderon in its maximal form".

In our fitting procedure we checked up such a possibility and made the fit with two intercepts. As a result we obtained the Odderon intercept  $\alpha_{0-Odd} - 1 = 0.1101 \pm 0.0004$  (with fixed Pomeron intercept  $\alpha_{0-Pom} - 1 = 0.11$ ), and that  $\chi^2$  did not practically changes. Hence, this confirms our assumption about the equality of both intercepts.

The second important assumption is that we choose the slope of the second term four times smaller than the slope of the first term, by analogy with the two pomeron cuts. An estimation of the diffraction slope of the generalized BFKL pomeron was made in [68] in terms of the correlation radius for the perturbative gluons. They show that indeed the pomeron trajectory has the finite slope  $\alpha'_{IP} \sim R_c^2$ , where  $R_c$  is the correlation radius for the perturbative gluons. They note that in the gBFKL dynamics a dimensionful  $\alpha'_{IP}$  is a nonperturbative quantity related to the nonperturbative infrared parameter of the model - the gluon propagation radius  $Rc$ . For the preferred  $Rc = 0.27 \text{ fm}$ , quite a small  $\alpha'_{IP} = 0.072 \text{ GeV}^2$  is found. In our work we used the phenomenological properties of the Pomeron (Odderon) taking into account that the Odderon only feels the centre of the proton and not the pion cloud. Therefore, it is reasonable to assume that the Odderon slope,  $B_{Odd}$ , is lower than that for the even-signature (Pomeron) amplitude [67]. This takes into account the data of the ISR experiments which show that the slope of the differential cross sections after the second bump is approximately four times smaller than the slope at small  $t$  as well as the conclusion of P. Landshoff that the Odderon contributions are essentially important at large momentum transfer. Our fitting procedure confirms also such assumption when we take the second slope as a free parameter.

##### B. Form factors

Since nucleons are not point particles, their structure must be taken into account. Usually, especially in the 60s - 70s, the researchers proposed that the hadron form factor is proportional to the charge distribution into the hadron, which can be obtained from electron-nucleon scattering.

This is primarily due to the electromagnetic structure of the nucleon which can be obtained from the electron-hadron elastic scattering. In the Born approximation, the Feynman amplitude for the elastic electron-proton scattering is

$$M_{ep \rightarrow ep} = \frac{1}{q^2} [e\bar{u}(k_2)\gamma^\mu u(k_1)][e\bar{U}(p_2)\Gamma_\mu(p_1, p_2)U(p_1)], (16)$$

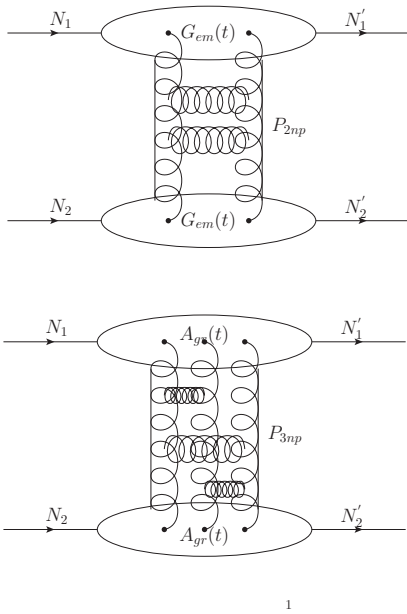


FIG. 4. The Born amplitudes of nucleon-nucleon elastic scattering: (top) with two non-perturbative gluons -  $P_{2np}$  and (bottom) three non-perturbative gluons -  $P_{3np}$ .

where  $u$  and  $U$  are the electron and nucleon Dirac spinors,

$$\Gamma^\mu = F_1(t)\gamma^\mu + F_2(t)\frac{i\sigma^{\mu\nu}q_\nu}{2m}, \quad (17)$$

where  $m$  is the nucleon mass,  $\kappa$  is the anomalous part of the magnetic moment and  $t = -q^2 = -(p - p')^2$  is the square of the momentum transfer of the nucleon. The functions  $F_1(t)$  and  $F_2(t)$  are named the Dirac and Pauli form factors, which depend upon the nucleon structure.

However, it is not obvious that strong interactions have to be proportional to the electromagnetic properties of hadrons. Taking into account this fact in one of the famous models, Bourrely-Soffer-Wu [69] used some modification of the form factor with free parameters which was obtained from the description of the differential cross section of hadron scattering. For example, it takes the form

$$G(t) = \frac{1}{1 - t/m_1^2} \frac{1}{1 - t/m_2^2} \frac{a^2 + t}{a^2 - t}. \quad (18)$$

However, this allows some freedom in the  $t$ -dependence of the scattering amplitude. It is necessary to take into account the parton distribution (PDFs) in the hadrons. However, PDFs depend on the Bjorken variable  $x$ . In the 80s some relations between PDFs and hadron form factor were proposed.

Note that the function like GPDs( $x, t, \xi = 0$ ) was used already in the old "Valon" model proposed by Sanevich and Valin in 1986 [70]. In the model, the hadron elastic form factor was obtained by the integration function  $L(x)G(x, t)$  where  $L(x)$  corresponds to the parton function and  $G(x, t)$  corresponds to the additional function which depends on momentum transfer and  $x$ . In modern

language,  $L(x)G(x, t)$  exactly corresponds to the GPDs. The scattering amplitude is

$$M_{AB}(s, t) = K_A(q^2)K_B(q^2)V(s, q^2); \quad (19)$$

where  $V(s, q^2)$  is a potential of strong interaction and  $K_{AB}(q^2)$  are the corresponding form factors.

$$K_p(q^2) = \frac{1}{3} \int_0^1 dx [2L_p^{u,d}(x)T_p^{u,d}(\vec{k})]; \quad (20)$$

where  $\vec{k} = (1-x)\vec{q}$ ,  $k^2 = (1-x)^2q^2$  and

$$T_p^u(\vec{k}) = e^{6.1k^2}; T_p^d(\vec{k}) = e^{3k^2}$$

. This form factor can be obtained taking into account PDF of interacting particles which is multiplied by some function depending on momentum transfer  $t$  and Boirken variable  $x$ .

Many different forms of the  $t$ -dependence of GPDs were proposed [71]. In the quark di-quark model [72] the form of GPDs consists of three parts - PDFs, function distribution and Regge-like function. In other works (see e.g. [73]), the description of the  $t$ -dependence of GPDs was developed in a more complicated picture using the polynomial forms with respect to  $x$ .

Commonly, the form of  $GPDs(x, \xi, t)$  is determined through the exclusive deep inelastic processes of type  $\gamma^*p \rightarrow Vp$ , where  $V$  stands for a photon or a vector meson. However, such processes have a narrow region of momentum transfer and in most models the  $t$ -dependence of GPDs is taken in factorization form with the Gaussian form of the  $t$ -dependence. Really, this form of  $GPDs(x, \xi, t)$  can not be used to build a space structure of hadrons, as for that one needs to integrate over  $t$  in a maximally wide region.

The conjunction between the momentum transfer and the impact parameter allows one to obtain a space parton distribution that has probability conditions [11]. The connections between the deep-inelastic scattering, from which we can obtain the  $x$ -dependence of parton distributions, and the elastic electron-nucleon scattering, where the form factors of the nucleons are obtained, can be derived by using the sum rules [17-20]. The form factors, which are obtained in different reactions, can be calculated as the Mellin moments of GPDs. Using the electromagnetic (calculated as the zero Mellin moment of GPDs) and gravitomagnetic form factors (calculated as the first moment of GPDs) in the hadron scattering amplitude, one can obtain a quantitative description of hadron elastic scattering in a wide region of energy and transfer momenta.

The proton and neutron Dirac form factors are defined as

$$\begin{aligned} F_1^p(t) &= e_u F_1^u(t) + e_d F_1^d(t), \\ F_1^n(t) &= e_u F_1^d(t) + e_d F_1^u(t), \end{aligned} \quad (21)$$

where  $e_u = 2/3$  and  $e_d = -1/3$  are the relevant quark electric charges. As a result, the  $t$ -dependence of the

$GPDs(x, \xi = 0, t)$  can be determined from the analysis of the nucleon form factors for which experimental data exist in a wide region of momentum transfer. This is a unique situation as it unifies elastic and inelastic processes.

In the limit  $t \rightarrow 0$ , the functions  $H^q(x, t)$  are reduced to usual quark densities in the proton:

$$\mathcal{H}^u(x, t = 0) = u_v(x), \quad \mathcal{H}^d(x, t = 0) = d_v(x)$$

with the integrals

$$\int_0^1 u_v(x) dx = 2, \quad \int_0^1 d_v(x) dx = 1$$

normalized to the number of  $u$  and  $d$  valence quarks in the proton. The energy-momentum tensor  $T_{\mu\nu}$  [18, 19, 21, 74] contains three gravitation form factors (GFF)  $A^{Q,G}(t)$ ,  $B^{Q,G}(t)$ , and  $C^{Q,G}(t)$ . We will scrutinize the first one which corresponds to the matter distribution in a nucleon. This form factor contains the quark and gluon contributions

$$A^{Q,G}(t) = A_q^{Q,G}(t) + A_g^{Q,G}(t).$$

To obtain the true form of the proton and neutron form factors, it is important to have the true form of the momentum transfer dependence of GPDs. Let us choose the  $t$ -dependence of GPDs in a simple form  $\mathcal{H}^q(x, t) = q(x) \exp[a_+ f(x) t]$ , with  $f(x) = (1-x)^2/x^\beta$  [75]. The isotopic invariance can be used to relate the proton and neutron GPDs; hence, we have the same parameters for the proton and neutron GPDs.

The complex analysis of the corresponding description of the electromagnetic form factors of the proton and neutron by different PDF sets (24 cases) was carried out in [76]. These PDFs include the leading order (LO), next leading order (NLO) and next-next leading order (NNLO) determination of the parton distribution functions. They used different forms of the  $x$  dependence of PDFs. We slightly complicated the form of GPDs in comparison with the equation used in [75], but it is the simplest one as compared to other works

$$\begin{aligned} \mathcal{H}^u(x, t) &= q(x)^u e^{2a_H f(x)_u t}, \\ \mathcal{H}_\Gamma^d(x, t) &= q(x)^d e^{2a_H f_d(x) t}, \end{aligned} \quad (22)$$

$$\begin{aligned} \mathcal{E}^u(x, t) &= q(x)^u (1-x)^{\gamma_u} e^{2a_E f(x)_u t}, \\ \mathcal{E}_\Gamma^d(x, t) &= q(x)^d (1-x)^{\gamma_d} e^{2a_E f_d(x) t}, \end{aligned} \quad (23)$$

where

$$f_u(x) = \frac{(1-x)^{2+\epsilon_u}}{(x_0+x)^m}, \quad f_d(x) = (1+\epsilon_0) \left( \frac{(1-x)^{1+\epsilon_d}}{(x_0+x)^m} \right).$$

The hadron form factors will be obtained by integration over  $x$  in the whole range of  $x$  - (0 - 1). Hence, the obtained form factors depend on the  $x$ -dependence of the forms of PDF at the ends of the integration region. The Collaborations determined the PDF sets from the inelastic processes only in some region of  $x$ , which is

only approximated to  $x = 0$  and  $x = 1$ . Some PDFs have the polynomial form of  $x$  with different power. Others have the exponential dependence of  $x$ . As a result, the behavior of PDFs, when  $x \rightarrow 0$  or  $x \rightarrow 1$ , can impact the form of the calculated form factors.

In that work, 24 different PDF were analyzed. On the basis of our GPDs with, for example, the PDFs ABM12 [77], we calculated the hadron form factors by the numerical integration and then by fitting these integral results by the standard dipole form with some additional parameters

$$F_1(t) = (4m_p - \mu t)/(4m_p - t) \tilde{G}_d(t),$$

with

$$\tilde{G}_d(t) = 1/(1 + a_1 q + q^2/a_2^2 + a_3^3 q^3)^2$$

which is slightly different from the standard dipole form by two additional terms with small sizes of coefficients ( $a_1 = 0.06$ ,  $\text{GeV}^{-1}$ ,  $a_2^2 = 0.78$   $\text{GeV}^2$ , and  $a_3^3 = 0.08$   $\text{GeV}^{-3}$ ). The matter form factor

$$A(t) = \int_0^1 x dx [q_u(x) e^{2\alpha_H f(x)_u/t} + q_d(x) e^{2\alpha_H f_d(x)/t}] \quad (24)$$

is fitted by the simple dipole form  $A(t) = \Lambda^4/(\Lambda^2 - t)^2$  with  $\Lambda^2 = 1.6$   $\text{GeV}^2$ . These form factors will be used in our model of proton-proton and proton-antiproton elastic scattering and further in one of the vertices of pion-nucleon elastic scattering.

To check the momentum dependence of the spin-dependent part of GPDs  $E_{u,d}(x, \xi = 0, t)$ , we can calculate the magnetic transition form factor, which is determined by the difference of  $E_u(x, \xi = 0, t)$  and  $E_d(x, \xi = 0, t)$ . For the magnetic  $N \rightarrow \Delta$  transition form factor  $G_M^*(t)$ , in the large  $N_c$  limit, the relevant  $GPD_{N\Delta}$  can be expressed in terms of the isovector GPD yielding the sum rules [21]

The experimental data exist up to  $-t = 8$   $\text{GeV}^2$  and our results show a sufficiently good coincidence with experimental data. It is confirmed that the form of the momentum transfer dependence of  $E(x, \xi, t)$  determined in our model is right.

Now let us calculate the moments of the GPDs with inverse power of  $x$ . This gives us the Compton form factors. The results of our calculations of the Compton form factors coincide well with the existing experimental data.  $R_V(t)$  and  $R_T(t)$  have a similar momentum transfer dependence but differ essentially in size. On the contrary, the axial form factor  $R_A$  has an essentially different  $t$  dependence.

A good description of the variable form factors and elastic scattering of hadrons gives large support to our determination of the momentum transfer dependence of GPDs. Based on this determination of GPDs, one can calculate the gravitomagnetic radius of the nucleon using the integral representation of the form factor and



make the numerical differentiation over  $t$  as  $t \rightarrow 0$ . This method allows us to obtain a concrete form of the form factor by fitting the result of the integration of the GPDs over  $x$ . As a result, the gravitomagnetic radius is determined as

$$\langle r_A^2 \rangle = -\frac{6}{A(0)} \frac{dA(t)}{dt} \Big|_{t=0}; \quad (25)$$

We used the same procedure as for our calculations of the matter radius. As a result, the Dirac radius is determined from the zero Mellin moment of GPDs

$$\langle r_D^2 \rangle = -\frac{6}{F(0)} \frac{dF(t)}{dt} \Big|_{t=0}; \quad (26)$$

where  $F(t) = \int_0^1 (e_u q_u(x) + e_d q_d(x)) e^{-\alpha t f(x)} dx$ .

One can obtain gravitational form factors of quarks, which are related to the second moments of GPDs. For  $\xi = 0$ , one has

$$\int_0^1 dx x \mathcal{H}_q(x, t) = A_q(t); \quad \int_0^1 dx x \mathcal{E}_q(x, t) = B_q(t). \quad (27)$$

The parameters of the phenomenological form of GPDs can be obtained from the analysis of the experimental data for the proton and neutron electromagnetic form factors simultaneously. Our determination of the momentum transfer dependence of GPDs of hadrons allows us to obtain good quantitative descriptions of different form factors, including the Compton, electromagnetic, transition, and gravitomagnetic form factor simultaneously.

## V. MODEL APPROXIMATION AND THE STRUCTURE OF THE ELASTIC SCATTERING AMPLITUDE

The differential cross sections of nucleon-nucleon elastic scattering can be written as a sum of different helicity amplitudes:

$$\frac{d\sigma}{dt} = \frac{2\pi}{s^2} (|\Phi_1|^2 + |\Phi_2|^2 + |\Phi_3|^2 + |\Phi_4|^2 + 4|\Phi_5|^2). \quad (28)$$

and the spin correlation parameter  $A_N(s, t)$  is

$$A_N \frac{s^2}{4\pi} \frac{d\sigma}{dt} = -[Im(\Phi_1(s, t) + \Phi_2(s, t) + \Phi_3(s, t) - \Phi_4(s, t)) \Phi_5^*(s, t)] \quad (29)$$

The HEGS model [33, 34] takes into account all five spiral electromagnetic amplitudes. The electromagnetic amplitude can be calculated in the framework of QED. For the spin-flip amplitudes, with the electromagnetic and hadronic interactions included, every amplitude  $\Phi_i(s, t)$  can be described as

$$\Phi_i(s, t) = \Phi_i^{em} \exp(i\alpha\varphi(s, t)) + \Phi_i^h(s, t), \quad (30)$$

where  $\varphi(s, t) = \varphi_C(t) - \varphi_{Ch}(s, t)$ , and  $\varphi_C(t)$  are calculated in the second Born approximation in order to allow the evaluation of the Coulomb-hadron interference term  $\varphi_{Ch}(s, t)$ . The quantity  $\varphi(s, t)$  has been calculated at a large momentum transfer including the region of the diffraction minimum [78, 79].

In the standard perturbative picture the spin-flip amplitudes die with growing of energy. However, there are different non-perturbative approaches which show non-dying spin-flip amplitudes, for example, [22–25] One of these is by E. Kuraev's [104, 105], which we used for our non-dying part of the spin-flip amplitude. We used also the second part of the spin-flip amplitude which has a Regge form (eq.50) and has the energy dependence of order  $1/s$ .

### A. Electromagnetic amplitudes and phase factor

The electromagnetic amplitude can be calculated in the framework of QED in the one-photon approximation

$$\begin{aligned} \Phi_1^{em}(t) &= \alpha f_1^2 \frac{s - 2m^2}{t}, \quad \Phi_3^{em}(t) = \Phi_1^{em}(t), \\ \Phi_2^{em}(t) &= \alpha \frac{f_2^2(t)}{4m^2}, \quad \Phi_4^{em}(t) = -\phi_2^{em}(t), \\ \Phi_5^{em}(t) &= \alpha \frac{s}{2m\sqrt{|t|}} f_1^2. \end{aligned} \quad (31)$$

The Coulomb-hadron interference phase is calculated with the dipole electromagnetic form factor [79]. For calculation of the Coulomb-hadron phase we take the energy dependence of the slope in the form  $b_{sl} = 6 + 0.75 \ln(s)$ .

We take  $\Lambda^2 = 0.71$ ; and  $\gamma = .577215665$ .

$$\begin{aligned} \phi_a &= q^2(2\Lambda^2 + q^2)/\Lambda^4 \ln(\Lambda^2 + q^2)^2/(\Lambda^2 q^2); \\ \phi_b &= (\Lambda^2 + q^2)^2/(\Lambda^4(4\Lambda^2 + q^2)^2 q\sqrt{4\Lambda^2 + q^2}); \\ &(4\Lambda^4(\Lambda^2 + 7q^2) + q^4(10\Lambda^2 + q^2)) \ln(4\Lambda^2/(\sqrt{(4\Lambda^2 + q^2) + q^2})); \\ \phi_c &= (2\Lambda^4 - 17\Lambda^2 q^2 - q^4)/(4\Lambda^2 + q^2)^2; \end{aligned}$$

$$\begin{aligned} \phi_{1-3} &= \phi_a + \phi_b + \phi_c; \\ \phi_{CN} &= -\ln b_{sl} q^2/2. + \gamma + \ln(1 + 8/(b_{sl}\Lambda^2)) - \phi_{1-3} \end{aligned}$$

### B. The hadron scattering amplitude

Let us define the hadron spin-non-flip amplitude as

$$F_{nf}^h(s, t) = [\Phi_{1h}(s, t) + \Phi_{3h}(s, t)]/2; \quad (32)$$

At small momentum transfer in the CNI region, there are two contributions coming from the electromagnetic and the strong interactions.

On the one hand, the interference of such contribution gives the possibility to determine the size of the real part

of the scattering amplitude. On the other hand, to determine the form of the imaginary part of the hadronic amplitude, it is necessary to extract the Coulomb contribution and the interference term. As the electromagnetic amplitude and its main contribution as  $t \rightarrow 0$  are well known, the measure of experimental data at very small  $t$  gives the possibility to improve the normalization of the differential cross sections.

The existence of the different sets of experimental data also allows one to improve separate normalization of experimental data. To compare different sets, some independent basis is needed.

Let us take the calculations of the differential cross sections carried out in the framework of the new high energy generalized structure (HEGS) model [33, 34] as such a basis. The model has only a few free parameters and it quantitatively describes experimental data in a wide domain of the momentum transfer, including the data in the CNI region, in a very wide energy region (from  $\sqrt{s} = 6$  GeV up to LHC energies) simultaneously with the same numbering of the free parameters. The HEGS model assumes Born terms for the scattering amplitude which get unitarization via the standard eikonal representation to obtain the full elastic scattering amplitude.

The scattering amplitude has exact  $s \leftrightarrow u$  crossing symmetry as it is written in terms of the complexified Mandelstam variable  $\hat{s} = se^{-i\pi/2}$  that determines its real part. The scattering amplitude also satisfies the integral dispersion relation at large  $s$ . It can be thought of as the simplest unified analytic function of its kinematic variables connecting different reaction channels without additional terms for separate regions of momentum transfer or energy. Note that the model reproduces the diffraction minimum of the differential cross section in a wide energy region [80]. The HEGS model describes the experimental data at low momentum transfer, including the Coulomb-hadron interference region, and hence includes all five electromagnetic spin amplitudes and the Coulomb-hadron interference phase.

Let us determine the Born terms of the elastic nucleon-nucleon scattering amplitude using both (electromagnetic and gravitomagnetic) form factors

$$\begin{aligned} F_{Pom2}^{Born}(\hat{s}, t) &= h_{Pom2} G_{em}^2(t) F_a(\hat{s}, t); \\ F_{Pom3}^{Born}(\hat{s}, t) &= h_{Pom3} A_{gr}^2(t) F_b(\hat{s}, t); \\ F_{Odd3}^{Born}(\hat{s}, t) &= h_{Odd3} A_{gr}^2(t) F_b(\hat{s}, t); \end{aligned} \quad (33)$$

where  $F_a(\hat{s}, t)$  and  $F_b(\hat{s}, t)$  have the standard Regge form:

$$F_a(s, t) = \hat{s}^{\alpha_0 + \alpha_1 t}; F_{b,c}(s, t) = \hat{s}^{\alpha_0 + \alpha_2 t}, \quad (34)$$

with  $\hat{s} = s e^{-i\pi/2}/s_0$ ;  $s_0 = 4m_p^2$  GeV<sup>2</sup>. The intercept of all main parts of the scattering amplitudes  $1 + \alpha_0 = 1.11$  was chosen as arithmetic means from different works including those on inelastic scattering. Hence, at the asymptotic energy we have the universality of the energy behavior of the elastic hadron scattering amplitudes. The main part of the slope of the scattering amplitude has the

standard logarithmic dependence on the energy  $B(s) = \alpha_{1,2} \ln(\hat{s})$  with  $\alpha_1 = 0.24$  GeV<sup>-2</sup> and  $\alpha_2 = \alpha_1/4$  GeV<sup>-2</sup>. It is taken with some correction (eq. 15).

Both the hadron electromagnetic and gravitomagnetic form factors were used in the framework of the high energy generalized structure (HEGS) model of elastic nucleon-nucleon scattering. This allowed us to build the model with a minimum number of fitting parameters [33, 34, 81]. The Born term of the elastic hadron amplitude can now be written as

$$\begin{aligned} F_h^{Born}(s, t) &= h_1 G^2(t) F_a(s, t) (1 + r_1/\hat{s}^{0.5}) \\ &+ h_2 A^2(t) F_b(s, t) \\ &\pm h_{odd} A^2(t) F_b(s, t) (h_{as} + r_2/\hat{s}^{0.75})(-t)/(1 - r_d t), \end{aligned} \quad (35)$$

where both (electromagnetic and gravitomagnetic) form factors are used. The corresponding parameters are determined by the fitting procedure.

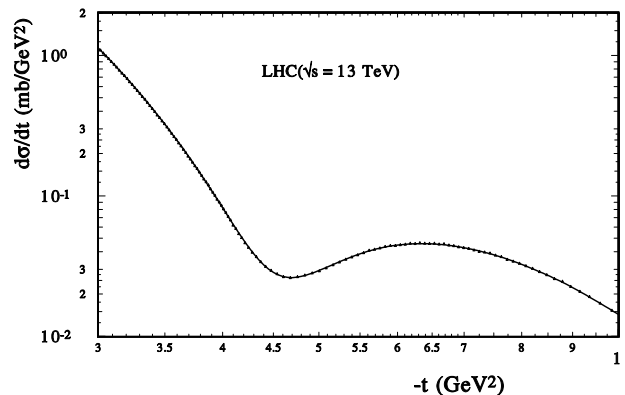


FIG. 5. The HEGS model calculation of  $d\sigma/dt$  of  $pp$  scattering at  $\sqrt{s} = 13$  TeV (points - experimental data of the TOTEM [27] Collaborations).

The final elastic hadron scattering amplitude is obtained after unitarization of the Born term [83]. There are some different approaches for summing the ladder diagrams - K-marix, U-matrix, standard eikonal, eikonal (with some inelastic corrections [85]). We analysed these forms and compared the results given by these approaches in some our works (for example, [82–84]). In most part, at high energy (especially at LHC energy) other approaches give worse results. Moreover, we introduced some parameters reflecting the Kaidalov corrections and obtained that their sizes are near zero or unity. So, this conserves the standard eikonal form. In a recent work [86] the authors compare the U-matrix with the eikonal and write in the conclusion "As it is seen in Fig.3 the eikonal approach better agrees with the ATLAS 13 TeV data."

So, we use the eikonal representation and at first, we

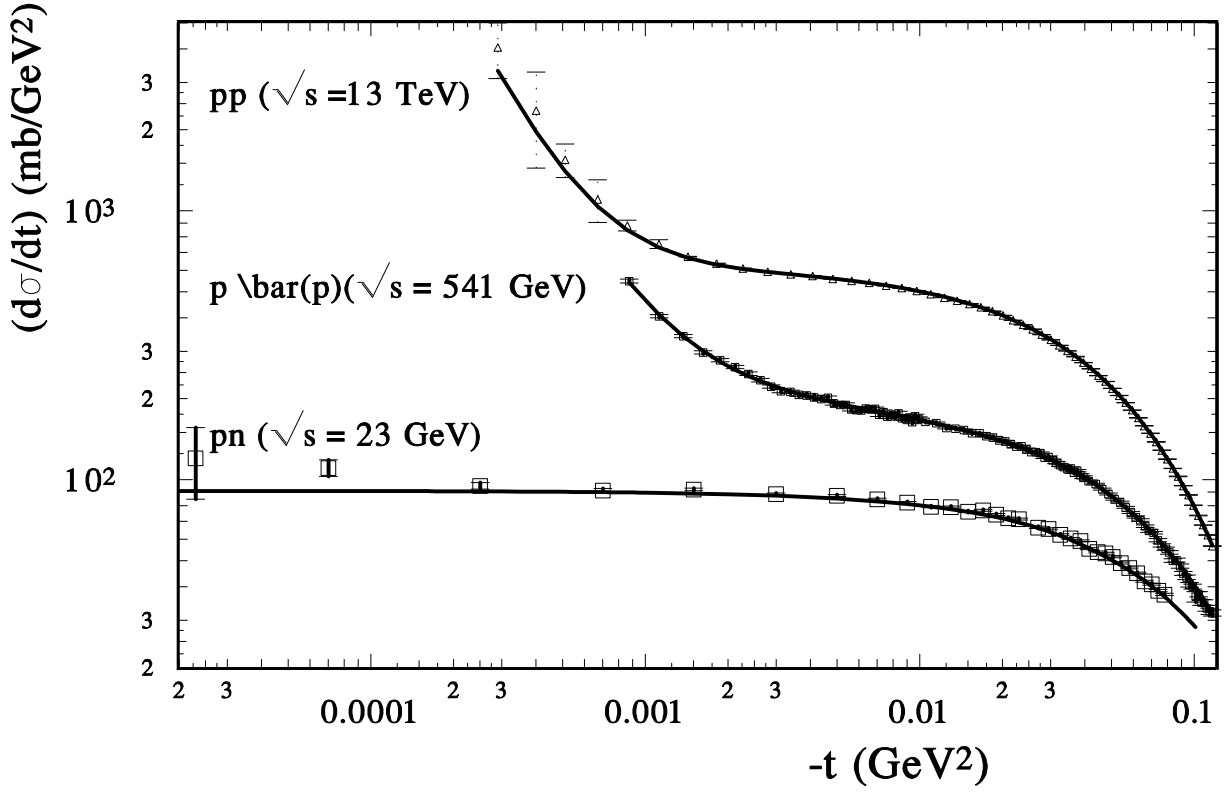


FIG. 6. The comparison of the HEGS model calculation of  $d\sigma/dt$  of  $pp$  scattering at  $\sqrt{s} = 13$  TeV (experimental data [60]),  $p\bar{p}$  scattering at  $\sqrt{s} = 53$  GeV (experimental data [61]) and  $pn$  scattering at  $\sqrt{s} = 23$  GeV (experimental data [61]).

have to calculate the eikonal phase

$$\chi(s, b) = -\frac{1}{2\pi} \int d^2q e^{i\vec{b}\cdot\vec{q}} F_h^{\text{Born}}(s, q^2)$$

and then to obtain the final hadron scattering amplitude

$$F_h(s, t) = is \int b J_0(bq) (1 - \exp[\chi(s, b)]) db.$$

The essential property of the model is that the real part of the scattering amplitude is obtained automatically through the complex  $\hat{s}$  only. The scattering amplitude has exact  $s \leftrightarrow u$  crossing symmetry.

So to extend the model to low energies, it is necessary to take into account the contributions of the second Regions. To avoid a substantially increasing number of fitting parameters, we introduce the effective terms which represent the contributions of the sums of different Regions. For the terms with the energy dependence order  $1/\sqrt{\hat{s}}$  we take for the  $pp$  scattering the cross even part in the form

$$F_{R1} = ih_{R1}/\sqrt{\hat{s}} e^{b_{R1}t \ln \hat{s}}, \quad (36)$$

and for the  $p\bar{p}$  the cross odd term in the form

$$F_{R1} = h_{R1}/\sqrt{\hat{s}} e^{b_{R1}t \ln \hat{s}} \quad (37)$$

where the value  $b_{R1}$  is fixed by unity. For the cross even part fast decreasing with growing energy, we take a term in the form

$$F_{R2} = h_{R2}/\hat{s} e^{b_{R2}t \ln \hat{s}}, \quad (38)$$

As a result, the low energy terms require only three additional fitting parameters.

The model is very simple from the viewpoint of the number of terms of the scattering amplitude and fitting parameters. There are no any artificial functions or any cuts which bound the separate parts of the amplitude by some region of momentum transfer. In the framework of the model, the description of experimental data was obtained simultaneously at the large momentum transfer and in the Coulomb-hadron region in the energy region from  $\sqrt{s} = 6$  GeV up to LHC energies. The model gives a very good quantitative description of the recent ex-

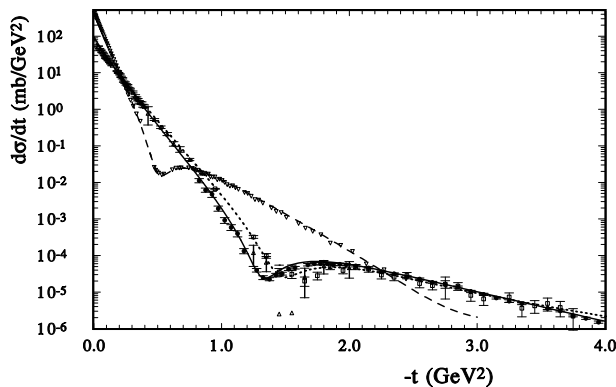


FIG. 7. The comparison of the HEGS model calculation of  $d\sigma/dt$  of  $pp$  scattering in the dip-bump regions at  $\sqrt{s} = 7$  TeV (dashed line and open triangles down),  $\sqrt{s} = 53.8$  GeV (solid line and circles) and at  $\sqrt{s} = 19.4$  GeV ( tiny dashed line and boxes).

perimental data at  $\sqrt{s} = 13$  TeV in the region of the diffraction minimum [31] (see Fig. 5).

As a result, good descriptions of the experimental data of  $pp$  and  $p\bar{p}$  elastic scattering (90 experimental sets including 4326 points and 256 polarization data) were obtained. Moreover a good description of  $pn$  data was also obtained. Some examples of such descriptions are presented in Fig. 5-7. Of particular interest is Fig. 6 where the comparison of the HEGS model calculation of  $d\sigma/dt$  of  $pp$  scattering at  $\sqrt{s} = 13$  TeV,  $p\bar{p}$  scattering at  $\sqrt{s} = 53$  GeV, and  $pn$  scattering at  $\sqrt{s} = 23$  GeV at small momentum transfer is shown. Practically for the first time, a simultaneous research of proton-proton, proton-antiproton and proton-neutron elastic scattering has been carried out in a wide energy (from 3.6 GeV up to 13 TeV) and momentum transfer region (from  $|t| = 2.10^{-4}$  GeV<sup>2</sup> up to  $|t| = 14$  GeV<sup>2</sup>).

In the fitting procedure based on the modern version of FUMILY [87, 88], we used only statistical errors. Systematic errors, which are mostly determined by indefiniteness of luminosity, were taken into account as an additional normalization coefficient, which is the same for all the data of a given set. The different normalization coefficients have practically random distributions. As a result, a wide range of possible forms of the scattering amplitudes prettily decreases.

A simultaneous description of the cross sections and spin correlation parameter of different nucleon-nucleon reactions, including 90 sets of experimental data, with the total number of data  $N = 4326$  gives a very reasonable  $\sum_{i,j} \chi_{i,j}^2 = 4826$ . The  $pn$  case with 526 experimental data, where the basic parameters were fixed from  $pp$  and  $p\bar{p}$  scattering,  $\sum_{i,j} \chi_{i,j}^2 = 585$ .

The data of the TOTEM at  $\sqrt{s} = 7$  TeV are consistent and their mean value is equal to 98.5 mb. The ATLAS Collaboration, using their differential cross section data in a region of  $t$  where the Coulomb-hadron interfer-

ence is negligible, obtained the value  $\sigma_{tot} = 95.35 \pm 2.0$  mb. The difference between the two results,  $\sigma_{tot}(s)(T.) - \sigma_{tot}(s)(A.) = 3.15$  mb, is about  $1 \sigma$ . At  $\sqrt{s} = 8$  TeV, the measured value of  $\sigma_{tot}$  grows, especially in the case of the TOTEM Collaboration, and the difference between the results of the two collaborations grows to  $\Delta(\sigma_{tot}(s)(T.) - \sigma_{tot}(s)(A.)) = 5.6$  mb, i.e.  $1.9 \sigma$ . This is reminiscent of the old situation with the measurement of the total cross sections at the Tevatron at  $\sqrt{s} = 1.8$  TeV via the luminosity-independent method by different collaborations.

Of course, we cannot say that the normalization of the ATLAS data is better than that of the TOTEM data simply because it coincides with the HEGS predictions. But this exercise may point to the main reason for the different values of the total cross sections obtained by the two collaborations. This does not exclude some further problems with the analysis of experimental data, e.g. those related to the analysis of the TOTEM data at  $\sqrt{s} = 7$  TeV [89].

One of the most important properties of the diffraction scattering is the form and energy dependence of the dip-bump structure. In Fig. 7, our model calculations are compared with the experimental data of  $pp$  scattering at ISR energies ( $\sqrt{s} = 19.4$  GeV and  $\sqrt{s} = 52.8$  GeV) and at the LHC energy  $\sqrt{s} = 7$  TeV and  $\sqrt{s} = 13$  TeV. At  $\sqrt{s} = 19.4$  GeV the real part of the  $pp$  scattering changes its sign at  $t = 0$  and we can see that it gives a small contribution to the diffraction minimum too. It is interesting that at  $\sqrt{s} = 13$  TeV the diffraction minimum has a sharp form either. The ratio of the maximum to minimum of the differential cross section at  $\sqrt{s} = 19.4$  GeV is 2.4 and equals 1.8 at the LHC energy. The position of the diffraction minimum  $t_{min}(s, t)$  moves to low momentum transfer continuously [80] and is described by the model very well (see, for example, Fig. 7 and Figs. 8,9,10 at low energies). It is interesting that the velocity of changing the position of the diffraction minimum changes very slowly. For example, from ISR energy  $\sqrt{s} = 53$  GeV up to SPS energy  $\sqrt{s} = 540$  GeV this position changes with a speed of 0.11 GeV<sup>2</sup> per 100 GeV. Between  $\sqrt{s} = 540$  GeV and  $\sqrt{s} = 7$  TeV such speed is two times less and equals 0.006, at last the position of minimum between 7 and 13 TeV changes with a speed of 0.002 per 100 GeV. The scaling of this process can approximately be represented as  $t_{min} \ln s/s_0 = const$ . After the second bump the slope of the differential cross sections increases with energy. It corresponds to the grows of the slope of the diffraction peak. In Figs. 7-9 the model calculations are compared with experimental data at low energies at small momentum transfer for  $pp$  and  $p\bar{p}$  scattering. It can be seen that the model reproduce well the existing experimental data of both reactions in that region.

The point of  $t$ , where the imaginary part changes its sign, determines the position of the diffraction minimum. But it moves slightly at some large  $t$  by the contribution of the real part of the elastic hadron scattering amplitude. The behavior of the imaginary part of the scattering amplitude over momentum transfer calculated in the

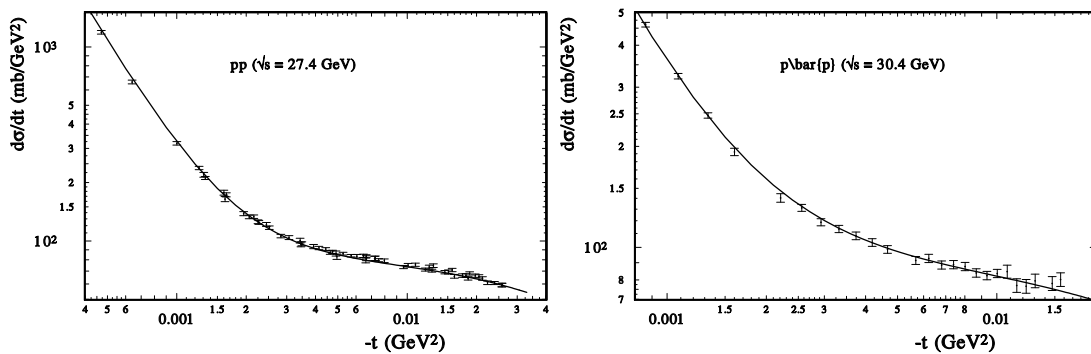


FIG. 8. The comparison of the HEGS model calculation of  $d\sigma/dt$  of  $pp$  scattering at  $\sqrt{s} = 27.4$  GeV [left]; and  $p\bar{p}$  scattering at  $\sqrt{s} = 30$  GeV [right].

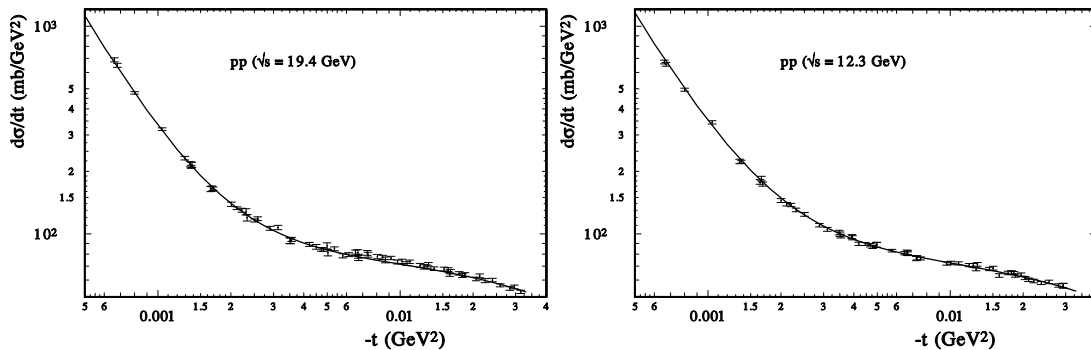


FIG. 9. The comparison of the HEGS model calculation of  $d\sigma/dt$  of  $pp$  scattering at  $\sqrt{s} = 19.45$  GeV [left]; and at  $\sqrt{s} = 12.3$  GeV [right].

framework of the HEGS model is presented in Fig. 11 for the energies  $\sqrt{s} = 0.51, 7, 13$  TeV. Again, we can see the point of crossover in the region of  $|t| = 0.2$  GeV<sup>2</sup>. Despite the essential growth of the size of the imaginary part of the scattering amplitude at a very small momentum transfer, its slope slightly changes with  $t$  in the region of the Coulomb nuclear interference. The size of the slope is practically proportional to the size of the total cross section in that region. However at larger  $t$ , for example at  $|t| = 0.1$  GeV<sup>2</sup>, it grows essentially faster.

It should be noted that the size of the slope of the differential cross sections is determined in that region of momentum transfer by the CNI interference term which is proportional to  $\alpha_{em}/t$  (where  $\alpha_{em}$  is a fine electromagnetic structure constant). It allows us to analyze [90] the first points of the unique experiment carried out by the ATLAS Collaboration [91].

The  $s$  dependence of the total cross sections of  $pp$  (solid line) and  $p\bar{p}$  (dashed line) scattering is shown in Fig. 12. The difference of the  $\sigma_{tot}^{p\bar{p}}$  and  $\sigma_{tot}^{pp}$  is less than 1 mb at  $\sqrt{s} = 20$  TeV.

### C. The real part of the elastic scattering amplitude

It is interesting that the form of the real part of the hadron elastic scattering amplitude is similar to its imaginary part. Of course, they are not proportional to each other as their connection has to satisfy the dispersion relations [30] which require, for example, the changing size of the real part at sufficiently small momentum transfer. In fact, in Fig. 14, we see that the real part changes its sign essentially earlier than the position of the diffraction minimum. At LHC energies this happens in the area of momentum transfer approximately equal to 0.2 GeV<sup>2</sup>. But before that, we can see the crossing point at  $|t| \sim 0.06$  GeV<sup>2</sup>. Likely, the behavior of the imaginary part the slope of the real part at very small momentum transfer is also practically proportional to the size of the total cross section at different energies and grows at larger momentum transfers. It can be seen that the real part at LHC energies has the negative maximum at approximately  $|t| = 0.3$  GeV<sup>2</sup> situated near the diffraction minimum. Hence, it essentially impacts the form and size of the diffraction minimum in the differential cross sections.

Especially the size and energy dependence of the real part of the hadronic amplitude impact the differential cross sections in the CNI region. The model descrip-

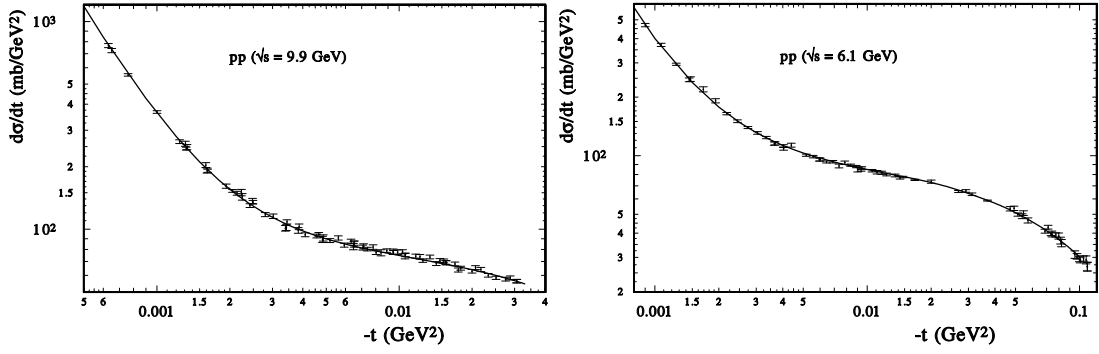


FIG. 10. The comparison of the HEGS model calculation of  $d\sigma/dt$  of  $pp$  scattering at  $\sqrt{s} = 9.9$  GeV [left]; and at  $\sqrt{s} = 6.1$  GeV [right].

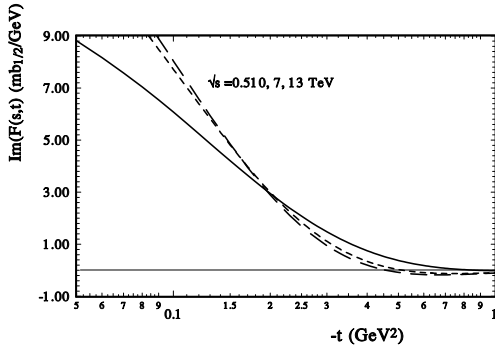


FIG. 11. The dependence of the imaginary part of the hadron scattering amplitude on  $s$  and  $t$  calculated in the model at the energy  $\sqrt{s} = 0.51, 7, 13$  TeV

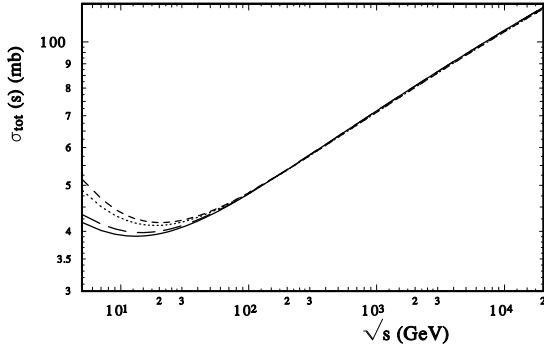


FIG. 12.  $\sigma_{tot}(s)$ : dashed line -  $p\bar{p}$  scattering, solid line -  $pp$  scattering; the same but without the second Reijons contributions (tiny dashed -  $p\bar{p}$  and long dashed  $pp$  scattering).

tions of the differential cross section at a small momentum transfer and at low energies are presented in Figures 5, 15-17. These figures show the experimental data with high precision and only statistical errors, which were taken into account in our fitting procedure. Obviously, the model reproduces the experimental data very well in a wide energy region.

One of the origins of the nonlinear behavior of the differential cross sections may be the different  $t$  dependen-

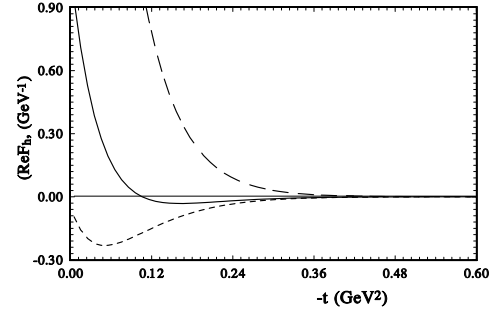


FIG. 13. The real part of the scattering amplitude coming from complex  $\hat{s}$  in the Regge representation (short dashed line - complex  $\hat{s}$  only in the exponential eq.(41); solid line full representation eq.(42)

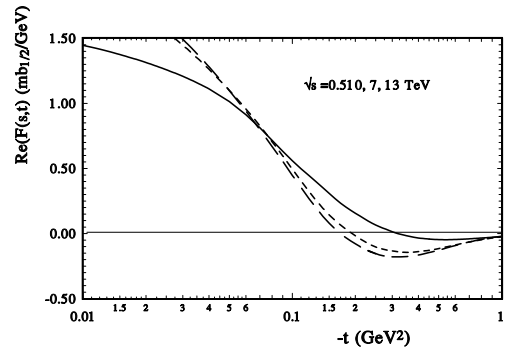


FIG. 14. The dependence of the real part of the hadron scattering amplitude on  $s$  and  $t$  calculated in the model at the energy  $\sqrt{s} = 0.51, 7, 13$  TeV

cies of the imaginary and real parts of the scattering amplitude. In most part, in different approaches it is supposed that this  $t$  dependence is the same for both parts of the scattering amplitude. It should be noted the importance of determining the size of the real part of the scattering amplitude was emphasized in many work of

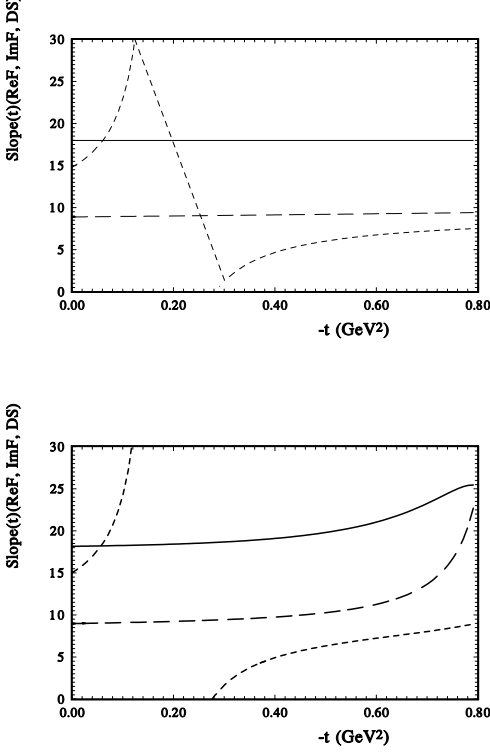


FIG. 15. The slopes of the Born term of the scattering amplitude [top] and the uniterized scattering amplitude [bottom] ( long dashed line -the slope of the imaginary part, the short-dashed line - the slope of the real part and the solid line - the slope of the differential cross sections.

Andre Martin. If at the LHC the value of  $\rho(s, t)$  is measured at high precision, it gives the possibility to check up the validity of the dispersion relations [56].

In the analysis of the experimental data [93] two cases were considered. One is the so-called "central" case, in which the ratio of the real to imaginary parts of the scattering amplitude is independent of momentum transfer or slightly decreases. The other, the so-called "peripheral" case, takes into account the assumption that  $\rho(s, t)$  grows with momentum transfer. Really, the last case contradicts the dispersion relations; hence, it has non-physical motivation.

Really, as the scattering amplitude has to be an analytic function of its kinematic variable, let us take the energy dependence of the scattering amplitude through the complex  $\hat{s} = se^{-i\pi/2}$ , and it must satisfy the dispersion relations.

For simplicity, very often they use the so-called local or derivative dispersion relations (see, for example, [45]) to determine the real part of the scattering amplitude.

For example, the COMPETE Collaboration used

$$ReF_+(E, 0) = \left(\frac{E}{m_p}\right)^\alpha \tan\left[\frac{\pi}{2}(\alpha - 1 + E \frac{d}{dE})\right] ImF_+(E, 0) / \left(\frac{E}{m_p}\right)^\alpha. \quad (39)$$

A different form of the derivative dispersion relation was taken as [92]

$$ReF_+(E, 0) = \left(\frac{\pi}{\ln(s/s_0)}\right) \frac{d}{d\tau} [\tau ImF_+(s, t) / Im_+(s, t = 0)] ImF_+(s, t = 0) \quad (40)$$

where  $\tau = t(\ln(s/s_0))^2$  and as  $s \rightarrow \infty$ . To satisfy these relations, the scattering amplitude has to be a unified analytic function of its kinematic variables connecting different reaction channels.

In most cases, one assumes that the real part is taken proportional to the imaginary part of the scattering amplitude. So the slopes of both parts are equal to each other. There is also some unusual assumption about the growth of the real part of the scattering amplitude at a small momentum transfer relative to its imaginary part (the so-called the peripheral case [93]). Obviously, both assumptions do not satisfy the dispersion relations, especially the last one.

Let us examine the origins of the complicated  $t$  dependence of the real part. Take the scattering amplitude in the form

$$F(s, t) = h s^\Delta e^{Bt \ln(\hat{s})}. \quad (41)$$

where the complex  $\hat{s}$  is used only in the exponential. In this case, the real part is negative (in Fig. 13, it is shown by the short dashed line) and essentially differs from the behavior of the imaginary part (long-dashed line). Now let us use  $\hat{s}$  in all parts of the scattering amplitude

$$F(s, t) = h \hat{s}^\Delta e^{Bt \ln(\hat{s})}. \quad (42)$$

The dispersion relations lead to the fact that the slope of the real part of the scattering amplitude must be

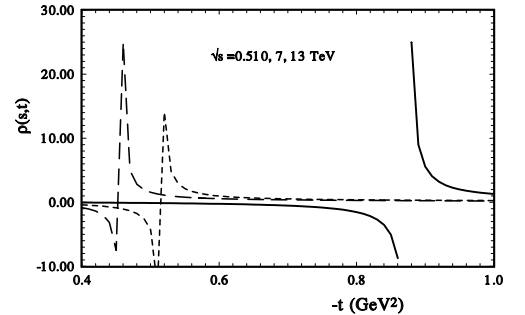


FIG. 16. The size of the  $\rho(s, t)$  - ratio of the real to imaginary part of the  $pp$  scattering amplitude is calculated in the model at the energy  $\sqrt{s} = 0.51, 7, 13 \text{ TeV}$  (solid, short dashed and dashed line respectively) depending on  $s$  and  $t$

larger than the slope of the imaginary part. For example, if the imaginary part of the spin-nonflip hadron elastic scattering amplitude takes a simple exponential form  $ImF_+ \sim he^{Bt}$ , then from eq.(40) we have that the real part of the  $F_+$  is  $ReF_+ = (1+Bt)e^{Bt}$ . Hence, it has zero in the region of momentum transfer around  $-0.1 - -0.15$   $GeV^2$

At last, but not least, it should be noted that the unitarization procedure has a strong influence on the  $t$  dependence of the real part of the scattering amplitude. For example, take the standard eikonal form of unitarization. If the Born term is taken in the ordinary exponential form (eq.42), then the imaginary part has a constant slope (see Fig. 15 [top]) and the real part has the first zero at a small momentum transfer. After eikonalization both slopes of the imaginary and real parts of the scattering amplitude have a strong  $t$  dependence (Fig. 15 [bottom]).

## VI. THE VALUE OF $\rho(s, t)$ AND ODDERON CONTRIBUTIONS

In Fig. 16, the ratio  $\rho(s, t)$  of the real to imaginary part of the hadron elastic scattering amplitude is presented for different energies. Such a complicated structure of  $\rho(s, t)$  is determined by the changes of the sign of the real and imaginary parts of the scattering amplitude. At a small momentum transfer, the size of  $\rho(s, t)$  is small as the real part changes its sign. Contrary, when the imaginary part changes its sign, the size of  $\rho(s, t)$  grows very faster. The energy dependence of  $\rho(s, t)$  is due to the movement of the position of the diffraction minimum, and hence to the energy dependence of the imaginary part of the scattering amplitude.

At high energies and in the region of small momentum transfer the difference between the  $pp$  and  $p\bar{p}$  differential cross sections comes in most part from the CNI term, as the real part of the Coulomb amplitude has a different sign in these reactions. In the standard fitting procedure, one neglects the  $\alpha_{em}^2$  term and then the equation takes the form:

$$d\sigma/dt = \pi[(F_C(t))^2 + (\rho(s, t)^2 + 1)(ImF_N(s, t))^2] + 2(\rho(s, t) + \alpha\varphi(t))F_C(t)ImF_N(s, t), \quad (43)$$

where  $F_C(t) = \mp 2\alpha G^2(t)/|t|$  is the Coulomb amplitude (the upper sign is for  $pp$ , the lower sign is for  $p\bar{p}$ ) and  $G^2(t)$  is the proton electromagnetic form factor squared;  $ReF_N(s, t)$  and  $ImF_N(s, t)$  are the real and imaginary parts of the hadron amplitude;  $\rho(s, t) = ReF_N(s, t)/ImF_N(s, t)$ . Formula (43) is often used for the fit of experimental data in getting hadron amplitudes and the Coulomb-hadron phase in order to obtain the value of  $\rho(s, t)$ . One can clearly see the impact of the value of  $\rho(s, t)$  on the form and energy dependence of the differential cross sections.

The Odderon amplitude has a large real part compared to its imaginary part. Hence, the odderon contribution

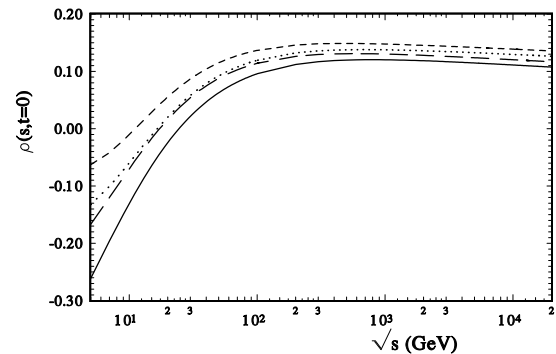


FIG. 17.  $\rho(s, t = 0)$ : dashed line -  $p\bar{p}$  scattering, solid line -  $pp$  scattering; the same but without the second Regions contributions (tiny dashed -  $p\bar{p}$  and long dashed  $pp$  scattering).

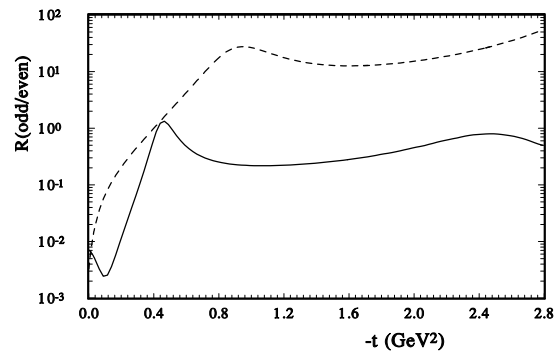


FIG. 18. The ratio  $R(s, t)$  of the cross-odd part of the scattering amplitude of elastic proton-proton scattering to its cross even part at 13 TeV (dashed line) and at 9.26 GeV (solid line).

changes the size and  $t$  dependence of the real part of the full amplitude. In a recent paper [94] different cases (with and without Odderon contributions) were analysed. It was noted that the effect of incorporating the Odderon becomes notably significant when analysing specific subsets of data. It is remarkable that the authors note "we will get too large  $\rho^{p\bar{p}}$  at  $\sqrt{s} \sim 541$  GeV in disagreement with the data UA4/2. As a result, they restored an old problem of the value of  $\rho(s, t)$  at  $\sqrt{s} \sim 540$  GeV. However, as was noted in the introduction, this problem strongly depends on the form of the non-linear slope and can be solved in [29, 95]. Now, in the present model, the Odderon amplitude essentially decreases as  $t \rightarrow 0$ . The value of  $\rho(\sqrt{s} = 541 \text{ GeV}, t = 0) = 0.122$ , which coincides with the result of the UA4/2 Collaboration.

In Fig. 18, the ratio of the cross-odd part of the scattering amplitude in the HEGS model of elastic proton-proton scattering to its cross even part at 13 TeV and at 9.26 GeV is presented. It is seen that this ratio is small at 13 TeV, except for the position of the diffraction minimum. At low energy, this ratio is small at small  $t$  but increases essentially in the region of a large momentum transfer.



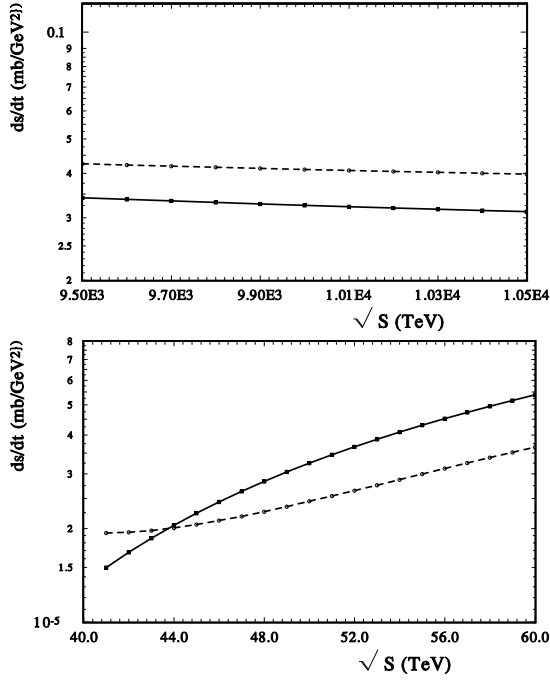


FIG. 19. The contributions of the Odderon part to the differential cross sections in the region of the dip a) [top]  $-t = 0.45 \text{ GeV}^2$ ; b) [down]  $-t = 1.45 \text{ GeV}^2$ .

However, the Odderon contribution is very important at the diffraction minimum. The real part of the scattering amplitude, which is positive at  $t = 0$  and  $\sqrt{s} > 30 \text{ GeV}$ , changes its sign at larger  $t$ , thus corresponding to the dispersion relations but, in any case, it fulfills the diffraction dip in the differential cross sections. Figure 17 shows the sizes of the differential cross sections in the region of the diffraction minimum with and without the Odderon contributions at  $\sqrt{s}$  around 53 GeV and at 10 TeV.

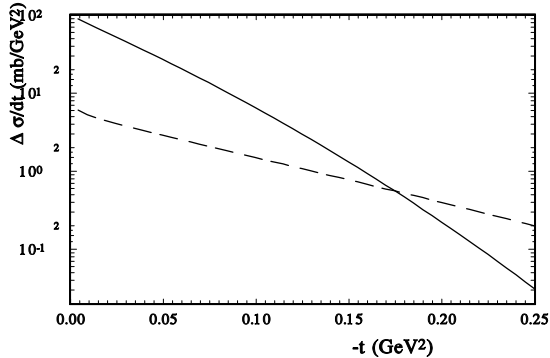


FIG. 20. The contributions  $\Delta(d\sigma/dt)$  of the anomalous term with a large slope to the differential cross sections of  $pp$  scattering at  $\sqrt{s} = 19 \text{ GeV}$  (solid line) and at  $\sqrt{s} = 13 \text{ TeV}$ .

## VII. NEW EFFECTS IN DIFFRACTION ELASTIC SCATTERING AT SMALL ANGLES

In the fitting procedure of the experimental data, only statistical errors were taken into account. As the systematic errors are mostly determined by indefiniteness of luminosity, they are taken into account as an additional normalization coefficient. This method essentially decreases the space of a possible form of the scattering amplitude. This allowed us to find the manifestation of small effects at 13 TeV experimental data for the first time [19-21]. Our further researches with taking into account a wider range of experimental data confirm the existence of such new effects. We determined the new anomalous term with a large slope as

$$f_{an}(t) = ih_{0an} \ln(\hat{s}/s_0)/k(1 + h_{1an} \ln(\hat{s}/s_0)/k) \exp[-\alpha_{an}(|t| + (2t)^2/t_n) \ln(\hat{s}/s_0)] G_{em}^2(t) \quad (44)$$

where  $h_{an}$  is the constant determining the size of the anomalous term with a large slope -  $\alpha_{an}$ ;  $G_{em}^2(t)$  is the electromagnetic form factor, which was determined from the GPDs [76], and  $k = \ln(13000^2 \text{ GeV}^2/s_0)$  is introduced for normalization of  $h_{an}$  at 13 TeV, and  $t_n = 1 \text{ GeV}^2$  is the normalization factor. This form adds only two additional fitting parameters, and this term is supposed to grow with energy of order  $\ln(\hat{s}/s_0)$ . The analysis of the data in a wide energy region gives a complicated energy dependence which is reflected in eq.(44). The term has a large imaginary part and a small real part determined by the complex  $\hat{s}$ . It is remarkable that the anomalous slope is determined with high accuracy  $\alpha_{an} = 0.513 \pm 0.004 \text{ GeV}^{-2}$  from the analysis of the whole sets of experimental data.

It is proportional to electromagnetic form factors, and the analysis of the experimental data above 6 GeV gives the size of the constant  $h_{an} = 1.13 \pm 0.04$ . It is a little less than obtained in the fit of only high energy data but now it has a more complicated energy dependence and a very small error. It impacts the differential cross sections at small  $t$  and the size of  $\sigma_{tot}(s)$ . However, it practically does not influence the value of  $\rho(s, t)$  as the imaginary and real parts of the scattering amplitude grow proportionally. The contributions of the anomalous term with a large slope to the differential cross sections of  $pp$  scattering -

$$\Delta(d\sigma/dt = d\sigma/dt|_{with} - d\sigma/dt|_{without})$$

are shown in Fig. 20 at  $\sqrt{s} = 19 \text{ GeV}$  (solid line) and at  $\sqrt{s} = 13 \text{ TeV}$  (dashed line). It can be seen that the contribution of the anomalous term disappears after  $-t > 0.2 \text{ GeV}^2$ . At low energies its relative contribution is less but remains visible and decreases with  $t$  slowly.

Our method helps us to find a small oscillation effect in the differential cross section at small momentum transfer [31]. Such oscillation can be determined by an additional oscillation term in the scattering amplitude [96]. The

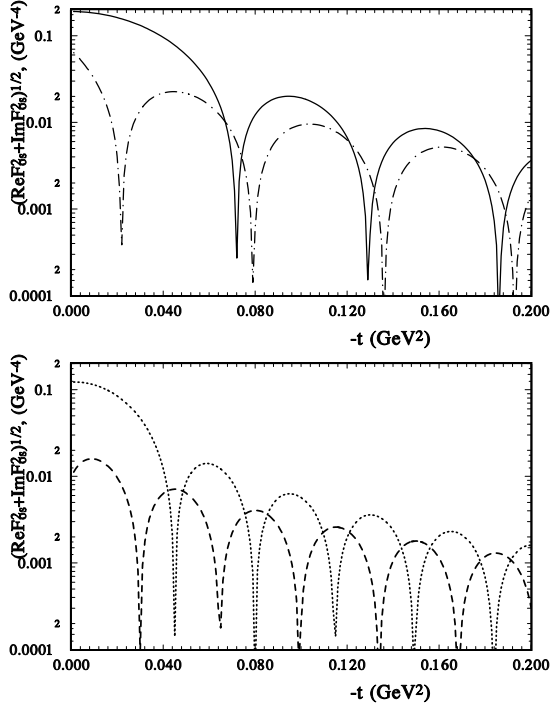


FIG. 21. The absolute value of the oscillation term  $(Re^2 F_{0s} + Im^2 F_{0s})^{1/2}$  at  $\sqrt{s} = 13$  TeV (solid line  $pp$  scattering; dashed points line -  $p\bar{p}$  scattering). and at  $\sqrt{s} = 540$  GeV (dotted line  $pp$  scattering; dashed line -  $p\bar{p}$  scattering)

theoretical predictions of some oscillations in the differential cross section has a long story, starting from one of the first paper [97] taking into account a multi pomeron exchange and the papers basing on the violation of the Pomernchuk theorem (for example, [6]) up to a recent paper [98]. In our fitting procedure the oscillatory function is

$$f_{osc}(t) = ih_{0osc}(1 \pm ih_{1osc}) \quad (45)$$

$$(\ln(\hat{s}/s_0)/k + h_s/\hat{s}) J_1(\tau)/\tau A^2(t),$$

$$\tau = \pi(\phi_0 - t)/t'_0;$$

here  $J_1(\tau)$  is the Bessel function of the first order;  $t_0 = 1/[a_p/(1 + 2 \ln^2(\hat{s}/s_0)/k)]$ , where  $a_p = 17.15 \text{ GeV}^{-2}$  is the fitting parameter that leads to the AKM scaling on  $\ln(\hat{s}/s_0)$ ;  $A(t)$  is the gravitomagnetic form factor, which was determined from the GPDs [76], and  $h_{osc}$  is the constant that determines the amplitude of the oscillatory term with the period determined by  $\tau$ . This form has only a few additional fitting parameters and allows one to represent a wide range of possible oscillation functions. The phase  $\phi_0$  is obtained near zero for  $pp$  scattering and it is slightly small and negative for  $p\bar{p}$  scattering, so it has a different sign for  $pp$  and  $p\bar{p}$  scattering. The inclusion of the  $p\bar{p}$  elastic scattering data in the fitting procedure

shows that part of the oscillation function changes its sign for the crossing reactions. As a result, the plus sign is related to  $pp$  and minus with  $p\bar{p}$  elastic scattering. Hence, this part is the crossing-odd amplitude, which has the same simple form for  $pp$  and  $p\bar{p}$  scattering only with a different sign.

The wider energy region used in this analysis allows one to reveal the logarithmic energy dependence of the oscillation term. The constant (size) of the oscillation function was determined from experimental data at high energies (all data above 500 GeV) as  $h_{osc}^c = 0.270 \pm 0.007 \text{ GeV}^{-2}$ , whereas in our analysis of the whole sets of the data  $\sqrt{s} > 3.6 \text{ GeV}$ . the  $h_{osc}^c = 0.232 \pm 0.009 \text{ GeV}^{-2}$ . The size of  $h_{osc}$  is obtained as is smaller than obtained in the only high energy data; however, the error is decreased essentially. Perhaps, this reflects a more complicated form of the energy dependence obtained now. Note, despite the logarithmic growth of the oscillation term, its relative contribution decreases as the main scattering amplitude grows as  $\ln^2(s)$ .

The oscillation term is represented in Fig. 21 at different energies  $\sqrt{s} = 13 \text{ TeV}$  and  $\sqrt{s} = 540 \text{ TeV}$  for the proton-proton and proton-antiproton scattering. It can be seen that the amplitude of the oscillation term increases at high energies, but the period of oscillations decreases with growing energy. Especially note that the period of oscillation is essentially less for  $p\bar{p}$  than for  $pp$  scattering. This can explain the difference which was noted in [99], in the behaviour of oscillations of the differential cross sections at  $\sqrt{s} = 540 \text{ GeV}$ , which were found in [100] and at  $\sqrt{s} = 13 \text{ TeV}$  [31]. Of course, the amplitude of oscillations is weak, so it is very difficult to identify it by experiment. However, our analysis of a wide energy region of experimental data gives a small error in the definition of the parameter determining the size of oscillations. This shows that further meticulous work is required, both from the theoretical and experimental points of view.

## VIII. PROTON-NEUTRON ELASTIC SCATTERING

We take in our analysis 24 sets of the proton-neutron experimental data from  $\sqrt{s} > 4.5 \text{ GeV}$  up to maximum energy  $\sqrt{s} > 27.5 \text{ GeV}$  where they correspond to experimental data with a total number of experimental points  $N = 526$ . As in the case of  $pp$  scattering, we include only statistical errors in our fitting procedure taking into account the systematic errors as additional normalization of a separate set. We take the amplitudes of the model obtained in the case of  $pp$  and  $p\bar{p}$  scattering and fix the parameters of the main terms and two anomalous terms, except for the terms of the second Reggions. The electromagnetic amplitudes are removed in this case. As a result, in the  $pn$  case, only the parameters of the second effective Reggion are obtained from the fitting procedure. Only in the Pomeron-neutron vertex  $F_{Pom2n}^{Born}$

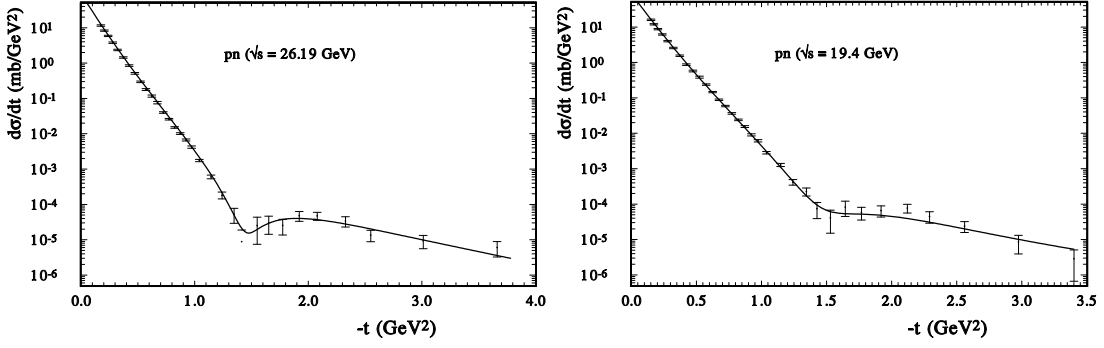


FIG. 22. The HEGS model calculation of  $d\sigma/dt$  of  $pn$  scattering [left] at  $\sqrt{s} = 26$  GeV; [right]  $\sqrt{s} = 19.4$  GeV.

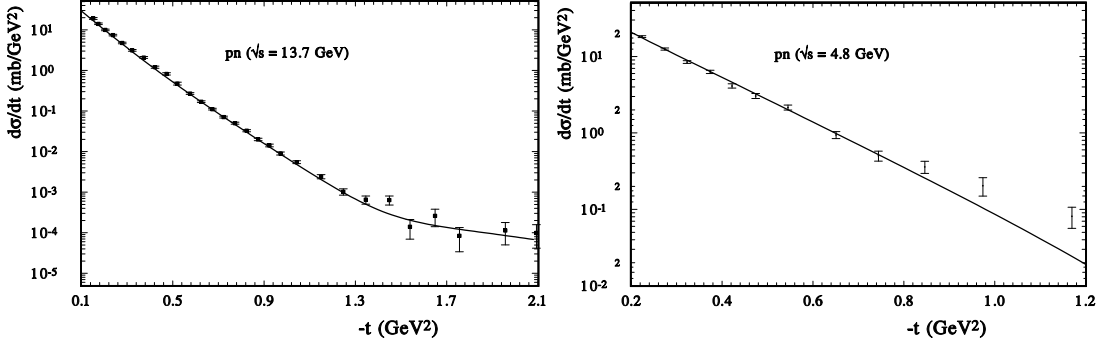


FIG. 23. The HEGS model calculation of  $d\sigma/dt$  of  $pn$  scattering [left] at  $\sqrt{s} = 13.7$  GeV; [right]  $\sqrt{s} = 4.8$  GeV.

is taken in the standard dipole form with free  $\Lambda_{pom-n}$ . Its value is obtained to be slightly above the standard electromagnetic  $\Lambda_{pom-n}^2 = 0.82$  GeV<sup>2</sup>. The obtained  $\sum_{i,j} \chi_{i,j}^2 = 567$ . The corresponding obtained description of the differential cross section is represent in Figs. 4, 21, 22. It is clear that the HEGS model works very well in the case of proton-neutron elastic scattering. In Fig. 22, the differential cross section of  $pn$  elastic scattering is represented for a large momentum transfer at energies  $\sqrt{s} = 26.19$  GeV and  $\sqrt{s} = 19.4$  GeV. At  $\sqrt{s} = 26.19$  GeV (Fig. 22[left]) the diffractive dip-bump structure is clearly represented whereas at  $\sqrt{s} = 19.4$  GeV (Fig. 22[right]) this structure is being leveled out and practically disappears at more lower energies (see Fig. 23). As in the case of  $pn$  scattering, there are many experimental data at small momentum transfer, where the contributions of our two anomalous terms are important; the successful description of the differential cross section confirms the existence of these terms.

### IX. POLARIZATION EFFECTS IN PROTON-PROTON ELASTIC SCATTERING

In the Regge limit  $t_{fix}$ . and  $s \rightarrow \infty$  one can write the Regge-pole contributions to the helicity amplitudes in the

$s$ -channel as

$$\Phi_{\lambda_1, \lambda_2, \lambda_3, \lambda_4}^B(s, t) \sim \sum_i g_{\lambda_1, \lambda_2}^i(t) g_{\lambda_3, \lambda_4}^i(t) [\sqrt{|t|}]^{|\lambda_1 - \lambda_2| + |\lambda_3 - \lambda_4|} \left(\frac{s}{s_0}\right)^{\alpha_i} (1 \pm e^{-i\pi\alpha_i}). \quad (46)$$

The corresponding spin-correlation values are presented in eq.(29).

Neglecting the  $\Phi_2(s, t) - \Phi_4(s, t)$  contribution, the spin correlation parameter  $A_N(s, t)$  can be written taking into account the phases of separate spin non-flip and spin-flip amplitudes as  $\varphi_{nf}(s, t)$ ,  $\varphi_{sf}(s, t)$  the analyzing power is

$$A_N(s, t) = -\frac{4\pi}{s^2} [(F_{nf}(s, t)) |F_{sf}(s, t)| \sin(\varphi_{nf}(s, t) - \varphi_{sf}(s, t))] / \frac{d\sigma}{dt}. \quad (47)$$

It is clearly seen that despite the large spin-flip amplitude, the analyzing power can be near zero if the difference of the phases is zero in some region of momentum transfer. The experimental data at some point of the momentum transfer show the energy independence of the size of the spin correlation parameter  $A_N(s, t)$ . Hence, the small value of the  $A_N(s, t)$  at some  $t$  (for example,

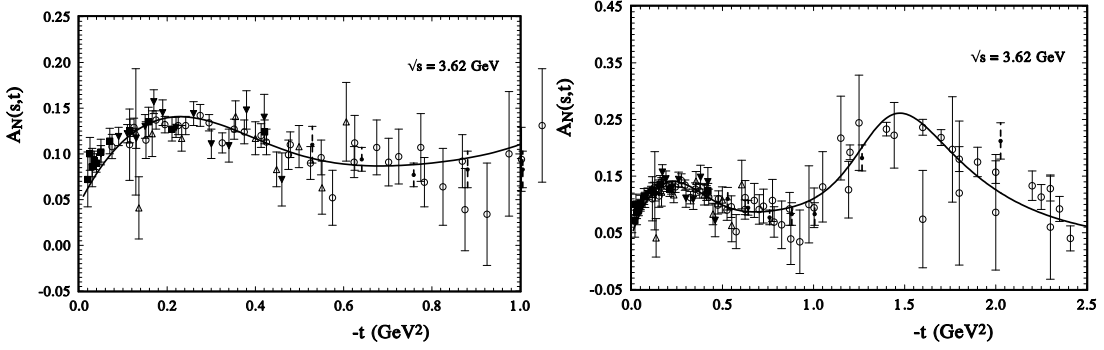


FIG. 24. The analyzing power  $A_N$  of pp - scattering is calculated: [left] at  $\sqrt{s} = 3.62$  GeV; (small  $t$ ), [right] (larger  $t$ ).

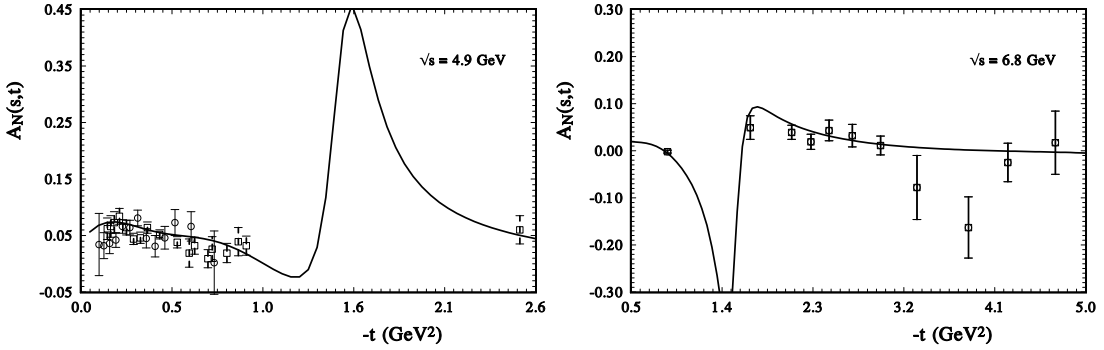


FIG. 25. The analyzing power  $A_N$  of pp - scattering calculated: [left] at  $\sqrt{s} = 4.9$  GeV, (the experimental data [61]), and [right] at  $\sqrt{s} = 6.8$  GeV (points - the experimental data [61]).

very small  $t$ ) does not serve as a proof that it will be small in other regions of momentum transfer.

It is usually assumed that the imaginary and real parts of the spin-non-flip amplitude have the exponential behavior with the same slope, and the imaginary and real parts of the spin-flip amplitudes, without the kinematic factor  $\sqrt{|t|}$  [101], are proportional to the corresponding parts of the non-flip amplitude. That is not so as regards the  $t$  dependence shown in Ref. [69], where  $F_h^{fl}$  is multiplied by a special function dependent on  $t$ . Moreover, one mostly takes the energy independence of the ratio of the spin-flip parts to the spin-non-flip parts of the scattering amplitude. All this is our theoretical uncertainty [102, 103].

In [104, 105], on the basis of generalization of the constituent-counting rules of the perturbative QCD, the proton current matrix elements  $J_p^{\pm\delta\delta}$  for a full set of spin combinations corresponding to the number of the spin-flipped quarks were calculated. This leads to part of the spin-flip amplitude

$$F_h^{sl} \sim \sqrt{-t}/(\frac{4}{9}m_p^2) \sqrt{-t}/(\frac{4}{9}m_p^2) \sqrt{-t}/(\frac{4}{9}m_p^2). \quad (48)$$

Hence, such an amplitude gives large contributions at large momentum transfer.

Of course, at lower energies we need to take into ac-

count the energy-dependent parts of the spin-flip amplitudes. So the form of the spin-flip amplitude is determined as

$$F_{sf1}(s, t) = ih_{sf1}q^3(1 + q^3/\sqrt{s})G_{em}^2e^{2tln\hat{s}} \quad (49)$$

We take the second part of the spin-flip amplitude in the form

$$F_{sf2}(s, t) = i\sqrt{|t|}G_{em}^2(h_5 + h_6(1 + ih_4)/ssc^2)e^{2tln\hat{s}} \quad (50)$$

This works in most part at low energies.

The minimal energy at which the analyzing power  $A_N(s, t)$  of pp - scattering examined in the HEGS model is  $\sqrt{s} = 3.62$  GeV. For our high energy model it is a very small energy. These results are shown in Fig. 24 at small  $t$  [left] and at larger  $t$  (right). These model calculations are compared with the results of four experiments. Obviously, we obtain a very good description of the experimental data. At these energies, the diffraction minimum is practically overfull by the real part of the spin-non-flip amplitude and the contribution of the spin-flip amplitude; however, the  $t$ -dependence of the analysing power is very well reproduced in this region of the momentum transfer.

Our calculation for  $A_N(t)$  is shown in Fig. 25 (left, right) at  $\sqrt{s} = 4.9$  GeV and  $\sqrt{s} = 6.8$  GeV. The description of the existing data is sufficiently good. Note

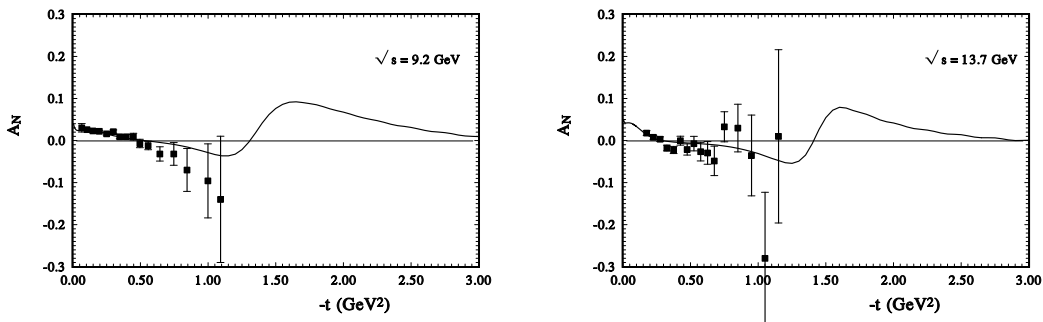


FIG. 26. The analyzing power  $A_N$  of pp - scattering calculated: [left] at  $\sqrt{s} = 9.2$  GeV (the experimental data [61]) and [right] at  $\sqrt{s} = 13.7$  GeV (points - the experimental data [61]).

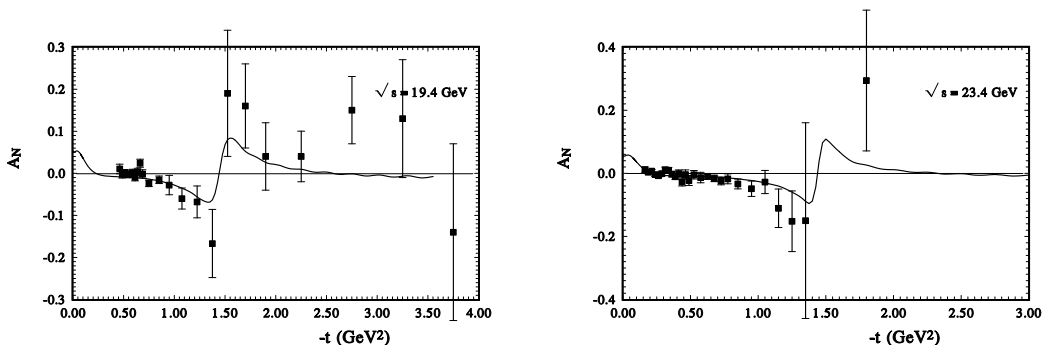


FIG. 27. The analyzing power  $A_N$  of pp - scattering calculated: [left] at  $\sqrt{s} = 19.4$  GeV (the experimental data [61]), and [right] at  $\sqrt{s} = 23.4$  GeV (points - the existing experimental data [61])

that the magnitude and the energy dependence of this parameter depend on the energy behavior of the zeros of the imaginary-part of the spin-flip amplitude and the real-part of the spin-nonflip amplitude. Figure 25 shows  $A_N(t)$  at  $\sqrt{s} = 9.2$  GeV and  $\sqrt{s} = 13.7$  GeV. At these energies the diffraction minimum deepens and its form affects the form of  $A_N(t)$ . At last,  $A_N(t)$  is shown at large energies  $\sqrt{s} = 19.4$  GeV and  $\sqrt{s} = 23.4$  GeV in Fig. 27. The diffraction dip in the differential cross section has a sharp form and it affects the sharp form of  $A_N(t)$ . The maximum negative values of  $A_N$  coincide closely with the diffraction minimum.

We have found that the contribution of the spin-flip to the differential cross sections is much less than the contribution of the spin-nonflip amplitude in the examined region of momentum transfers.  $A_N$  is determined in the domain of the diffraction dip by the ratio

$$A_N \sim \text{Im}f_- / \text{Re}f_+. \quad (51)$$

The size of the analyzing power changes from  $-45\%$  to  $-50\%$  at  $\sqrt{s} = 50$  GeV up to  $-25\%$  at  $\sqrt{s} = 500$  GeV.

These numbers give the magnitude of the ratio, eq.(51), that does not strongly depend on the phase between the spin-flip and spin-nonflip amplitudes. This picture implies that the diffraction minimum is mostly filled by the real-part of the spin-nonflip amplitude and that the imaginary-part of the spin-flip amplitude increases in this domain as well.

## X. CONCLUSIONS

Practically for the first time, a simultaneous research of proton-proton, proton-antiproton and proton-neutron elastic scattering has been carried out in a wide energy (from 3.6 GeV up to 13 TeV) and momentum transfer region (from  $|t| = 2.10^{-4}$  GeV<sup>2</sup> up to  $|t| = 14$  GeV<sup>2</sup>). In the fitting procedure we used only statistical errors. Systematic errors, which are mostly determined by indefiniteness of luminosity, take into account as additional normalization coefficient. As a result, a wide range of possible forms of the scattering amplitudes decrease con-

siderably. In this paper a simultaneous description of the cross sections and spin correlation parameter of different nucleon-nucleon reactions, including 90 sets of experimental data, with the total number of data  $N = 4326$  gives a very reasonable  $\sum_{i,j} \chi_{i,j}^2 = 4826$ . The  $pn$  case with 526 experimental data, where the basic parameters were fixed from  $pp$  and  $p\bar{p}$  scattering,  $\sum_{i,j} \chi_{i,j}^2 = 585$ .

Our analysis is carried out by using a successful development of the HEGS model which can be applied in a wide energy and momentum transfer regions. The model of hadron interaction is based on the analyticity of the scattering amplitude with taking into account the hadron structure, which is represented by GPDs. Different origins of the non-linear behavior of the slope of the scattering amplitude are analyzed. The possible contribution of a meson threshold is compared with different forms of the approximations for a non-linear slope at a small momentum transfer.

The relative contributions of the possible different part of the scattering amplitude were especially analyzed. It is remarkable that in the model the main pomeron and odderon amplitudes have the same intercept. After eikonalization this leads to the  $\ln^2(s)$  energy dependence. In this sense, we have some case of maximal Odderon. In the model, the odderon amplitude has a special kinematic factor and does not give a visible contribution at a zero momentum transfer.

It was found that the new anomalous term with a large slope has the complicated logarithmic energy dependence and has the cross even properties. Hence, it is part of the pomeron amplitude and is also proportional to charge distributions. Our analysis of the contribution of the so-called hard pomeron with a large intercept does not show a visible contribution of this term. The second additional term, which represents the additional oscillation properties of the scattering amplitude at a small momentum transfer with the cross-odd properties, has a logarithmic energy dependence and is proportional to the gravitomagnetic form factor. Hence, it belongs to the odderon contribution to the scattering amplitude.

As was noted in many models, the oscillations of the scattering amplitude are connected with the broken Pomanchuk theorem and the scattering amplitude grows to a maximal possible extent but not breaking the Froissart boundary. In our opinion that oscillation of the scattering amplitude is connected with the behavior of hadron interaction potential at large distances [31, 106, 107]. Note that in [108] a quark-antiquark potential as function of the separation distance  $r$  between

the particles for the perturbative case in the framework of the Refined Gribov-Zwanziger Model (RGZ) was calculated. It includes a combination of oscillating terms. This can be compared to the Perturbative approach at short distances and Lattice QCD in the IR regime. So the researches into the properties of the oscillations term can give a very important information about the hadron interactions at large distances. Of course, this requires further theoretical and experimental works.

This helps reduce some tension between the TOTEM and ATLAS data. No contribution is shown of hard-Pomeron to elastic hadron scattering. However, the importance of Odderon's contribution is shown. A good description of proton-neutron differential scattering with 526 experimental points including the experimental data which reach extremely small momentum transfer  $t = 2 \cdot 10^{-4} \text{ GeV}^2$  is also obtained on the basis of the amplitudes taken from the analysis of  $pp$  and  $p\bar{p}$  scattering. A good enough description of the polarization data was also obtained, which reflects the true phases of the spin-non-flip and spin-flip amplitudes, so the value of  $A_N(s, t) \sim \varphi_{sp-n-flip} - \varphi_{sp-flip}$ .

Our work supports that GPDs reflect the basic properties of the hadron structure and provide a bridge between many different reactions. The determined new form of the momentum transfer dependence of GPDs allows one to obtain different form factors, including Compton form factors, electromagnetic form factors, transition form factor, and gravitational form factors. The chosen form of the  $t$ -dependence of GPDs of the pion (the same as the  $t$ -dependence of the nucleon) allows us to describe the electromagnetic and gravitomagnetic form factors of pion and pion-nucleon scattering.

The impact of the different  $t$  dependence of the real and imaginary parts of the elastic scattering amplitude at small  $t$  should be noted. The dispersion relation shows that the real part has zero at small  $t$ , approximately in the domain  $-t = 0.1$ ; of course this depends on the energy. Hence, the contrary behavior of the real part (grows at small  $t$ , the so-called "peripheral case" of the phase of the scattering amplitude) which is examined in [36] has no physical meaning.

**Acknowledgement:** OVS would like to thank O. Teryaev and Yu. Uzikov for their kind and helpful discussion. This research was carried out at the expense of the grant of the Russian Science Foundation No. 23-22-00123, <https://rscf.ru/project/23-22-00123>.

- 
- [1] Bogolyubov N.N., Shirkov D.V. Quantum Fields. Benjamin-Cummings Pub. Co, (1982).  
 [2] H. Goodhew, S. Jazayeri, E. Pajer, // arXiv:20009.02898[hep-th].  
 [3] Yu.N. Uzikov and A.A. Temerbayev, Phys. Rev. C **2015**

- 92**, 014002-014009.  
 [4] A.F. Martin, and E. Predazzi, Phys. Rev. D **66** (2002) 034029.  
 [5] Roy S.M., *Phys.Lett.* **B 34**, 407 (1971).  
 [6] Auberson G., Kinoshita T., Martin A., *Phys. Rev.* **D3**,

- 3185 (1971).
- [7] J. Fischer, *Phys.Rep.* **76**, 157 (1981).
- [8] V.A. Petrov, V. A. Okorokov, *Int. J. Mod. Phys. A33*, 1850077 (2018)
- [9] I.M. Dremin, *Int. J. Mod. Phys. A*, **31**, 1650107 (2016).
- [10] I.M. Dremin, *Physics1*(1), 33 (2019).
- [11] M. Burkardt, *Phys. Rev.* **D62**, 2000, 071503 2
- [12] B. Duran et al., *Nature*, **615**, 813 (2023).
- [13] V. D. Burkert, L. Elouadrhiri and F. X. Girod, *Nature*, **557**, no.7705, 396 (2018).
- [14] O. V. Teryaev, *Front. Phys. (Beijing)* 11, 111207 (2016).
- [15] G. E. Dodge, *Nucl.Phys.News*, **34** 3 (2024).
- [16] V.V. Abramov et al., *PEPAN*, **52** 1392 (2021).
- [17] Müller et al., *Fortschr. Phys.*, 42 , 101, ( 1994).
- [18] X.D. Ji, *Phys. Lett.* **78** , (1997) 610;
- [19] X.D. Ji, *Phys. Rev D* 55, 7114 (1997).
- [20] A.V. Radyushkin, *Phys. Rev. D* **56**, (1997) 5524.
- [21] M. Guidal, M.V. Polyakov, A.V. Radyushkin, and M. Vanderhaeghen, *Phys. Rev. D* **72** , 054013 (2005) .
- [22] B.Z. Kopeliovich, B.G. Zakharov, *Phys. Lett. B* **156**, (1989).
- [23] M. Anselmino and S. Forte, *Phys. Rev. Lett.* **71**, 223 (1993).
- [24] S. V. Goloskokov, S. P. Kuleshov, O. V. Selyugin, "Spin Spin effects in high energy hadron-hadron scattering", *Z. Phys. C* **1991** 50, 455-464.
- [25] A.E. Dorokhov, N.I. Kochelev and Yu.A. Zubov, *Int. Jour. Mod. Phys.* **A8**, 603 (1993).
- [26] G. Antchev *et al.* [TOTEM Collaboration], arXiv:1812.04732 [hep-ex].
- [27] G. Antchev et all. (TOTEM Collaboration) *Eur.Phys.J.C* 79 (2019) 10, 861
- [28] E. Martynov, B. Nicolescu, *Phys. Lett. B* 778, 414, (2018) 414.
- [29] O. Selyugin, *Phys. Lett.* **B333**,(1994) 245.
- [30] Cudell J.R., Selyugin O.V., *Phys.Rev.Lett.* **102**, 032003 (2009).
- [31] O. V. Selyugin, *Phys.Lett.*, **B 797** 134870 (2019).
- [32] O. V. Selyugin, *Mod.Phys.Lett. A*, **36**, No. 18 (2021) 2150148.
- [33] O. V. Selyugin, *Eur. Phys. J. C* **72**, 2073 (2012).
- [34] O. V. Selyugin, *Phys. Rev. D* **91**, no. 11, 113003 (2015) Erratum: [*Phys. Rev. D* **92**, no. 9, 099901 (2015)].
- [35] R.G. Newton, book, McGraw-Hill Book Company (New York-San Francisco-St. Louis-Toronto-London-Sydney) (1980).
- [36] The TOTEM Collaboration (G. Antchev et al.) *Nucl. Phys. B*, **899**, 527 (2015).
- [37] G. Alberi, and G. Goggi, *Phys.Rep.* **74**, 1 (1981).
- [38] Yu.M. Antipov et al., Preprint IHEP (Protvino) 76-95 (1976).
- [39] O. V. Selyugin, O.V. Selyugin, *Int.workshop, Protvino* (1982).
- [40] J. Pumplin *Phys.Lett.*, **B 276** 517 (1992).
- [41] S. V. Goloskokov, S. P. Kuleshov and O. V. Selyugin, *Sov. J. Nucl. Phys.* **35**, 895 (1982) [*Yad. Fiz.* **35**, 1530 (1982)]; *Z. Phys. C* **50**, 455 (1991).
- [42] H. Cheng, an T.T. Wu, *Phys.Rev.Lett.*, **24** 1456 (1970).
- [43] J.L. Cardy, *Nucl. Phys.*, **B28**, 455, 477 (1971).
- [44] J.M. Schwarz, *Phys.Rev.*, **167**, 1342 (1968).
- [45] J.B. Bronzan, C.S. Hui, *Phys.Rev.* , **D4** , 964 (1972).
- [46] G. Cohen-Tannoudji, V.V. Ilyin, and L.L. Jenkovszky, *Lett.Nuovo Cim.*, **5** 957 (1972).
- [47] A.O.Barut and D.E. Zwanziger, *Phys.Rev.*, **127**, 974 (1962).
- [48] A.O.Barut, *Phys.Rev.*, **128**, 1383 (1963).
- [49] V.N. Gribov, *Nucl.Phys.* , **22**, 249 (1961).
- [50] V.N. Gribov and I.Ya. Pomeranchuk *Nucl.Phys.* , **38**, 516 (1962).
- [51] A. Anselm and V. Gribov, *Phys. Lett.* **B40**, 487 (1972).
- [52] V.A. Khoze, A.D. Martin and M.G. Ryskin, arxiv:hep-ph/0007359.
- [53] V.A. Khoze, A.D. Martin and M.G. Ryskin, arXiv:1410.0508.
- [54] Van Hove, lecture (1966).
- [55] S. Barshay, and Y.-A. Chao, *Phys.Rev. Lett.* **29** 753 (1972).
- [56] R. Fiore, L. Jenkovszky, R. Orava, E. Predazzi, A. Prokudin, O. Selyugin, *Mod.Phys.*, **A24**: 2551-2559 (2009)
- [57] A. Degasperis and E. Predazzi, *Nuovo Cim.* **A65** (1970) 764.
- [58] L.Jenkovsky, *Phys. Rev. D* **60** 074028 (1999) .
- [59] S. Trokenheim, *Fermilab-Thesis-1995-40*,(1995).
- [60] ATLAS Collaboration, *Eur. Phys. J. C* 83 (2023) 441.
- [61] Durham HepData Project, [http:// durpdg.dur.ac.uk/hepdata/reac.html](http://durpdg.dur.ac.uk/hepdata/reac.html).
- [62] Spires data-base.
- [63] K.R. Schubert, "Elastic and Inelastic Hadron Diffraction at High-Energies", *In Landolt-Bronstein, New Series, 1979, 1/9a*.
- [64] L. Lukaszuk, B. Nicolescu, *Lett. al Nuovo Cimento* 8 (1973), 405.
- [65] Y.V. Kovchegov and E. Levin, *Quantum Chromodynamics at High Energies*, Cambridge Monographs on Particle Physics, Nuclear Physics and Cosmology, Cambridge University Press, (2012).
- [66] G. Antchev et al.,TOTEM COLL., *Eur.Phys.J.C* 80 (2020) 2, 91.
- [67] V.A. Khoze, A.D. Martin, M.G. Ryskin, arxiv: 1801.07065.
- [68] N.N.Nikolaev, B.G.Zakharov, V.R.Zoller, *JETP Lett.* **60** (1994) 694-698).
- [69] C. Bourrely, J. Soffer and T. T. Wu, *Phys. Rev. D* **19**, 3249 (1979).
- [70] S. Sanielevici and P.Valin, *Phys.Rev.* **D29**, 52 (1984).
- [71] B. Kriesten, et all. *Phys. Rev. D* **101**, (2020) 054021.
- [72] J. Grigsby, B. Kriesten, J. Hoskins, S. Liuti, P. Alonzi, M. Burkardt, *Phys. Rev. D* **104**, (2021) 016001.
- [73] M.Diehl *et al.*, *Eur.Phys. J. C* **39** (2005)
- [74] H. Pagels, *Phys.Rev.* 144 (1966) 1250).
- [75] O. Selyugin, O. Teryaev, *Phys. Rev. D* **79** 033003 (2009);
- [76] O.V. Selyugin, *Phys. Rev. D* **89** 093007 (2014) .
- [77] S. Alekhin, J. Blu"mlein, and S. Moch, *Phys.Rev.* **D86** (2012) 054009.
- [78] O.V. Selyugin, *Mod. Phys. Lett.* **A9** (1994) 1207.
- [79] Selyugin O.V., *Phys. Rev. D* **60**, (1999) 074028-1 - 074028-9.
- [80] Selyugin O.V., *Nucl. Phys. A* **959** 116 (2017).
- [81] O. V. Selyugin, *Nucl.Phys. A* , **2013**, 903, 54-64.
- [82] O.V. Selyugin, *Phys.Lett.*, **B 662** (2008) 417.
- [83] J.-R. Cudell, E. Predazzi, and O.V. Selyugin, *Eur. Phys. J. A* **21** (2004); hep-ph/0401040.
- [84] J.-R. Cudell, E. Predazzi, and O.V. Selyugin, *Phys.Rev.* **D 79** , (2009) 034033.
- [85] A.B. Kaidalov, *Phys. Rep.* **50** (1979) 157.

- [86] E. G. S. Luna, M. G. Ryskin, arxiv-2408.00194.
- [87] I.M. Sitnik, *Comp.Phys.Comm.*, **185**, 599 (2014).
- [88] I.M. Sitnik, I.I. Alexeev, O.V. Selyugin, *Comp.Phys.Comm.*, **251**, 107202 (2020).
- [89] O. V. Selyugin, *Nucl. Phys. A* **922**, (2014) 180.
- [90] O.V. Selyugin, arXiv:2210.02970 [hep-ph].
- [91] ATLAS Collaboration, [arXiv:2207.12246; H. Stenzel et al. (ATLAS Collaboration), arxiv 2209.11.487
- [92] S. M. Roy, arXiv:1602.03627 [hep-ph].
- [93] G. Antchev *et al.* [TOTEM Collaboration], CERN-PH-EP-2015-325, arXiv:1610.00603 [nucl-ex].
- [94] E.G.S. Luna, M.G. Ryskin, V.A. Khoze, arXiv:2405.09385 [hep-ph].
- [95] O. V. Selyugin, *Sov. J. Nucl. Phys.* **55**, 466 (1992) [*Yad. Fiz.* **55**, 841 (1992)].
- [96] O. V. Selyugin, *Eur. Phys. J. C* **84** (2024) 649.
- [97] A.A. Anselm and I.T. Dyatlov, *Phys.Lett. B* **24** (1967) 479; *Yad.Fiz.* **9** (1969) 416.
- [98] P. Grafstrom, A. D. Martin, M. G. Ryskin, arXiv:2405.07802; IPPP/24/24, DCPT/24/48.
- [99] Grafstrom, arXiv: 2307.15445v1
- [100] P. Gauron, B. Nicolescu, O.V. Selyugin, *Phys. Lett. B* **390** (1997) 405.
- [101] N.H. Buttmore et al., *Phys.Rev. D* **59** (1999) 114010.
- [102] A.F. Martin, and E. Predazzi, *Phys. Rev. D* **66** (2002) 034029.
- [103] O.V. Selyugin, J.-R. Cudell, E. Predazzi, *Eur.Phys.J.ST* **162:37-42**,2008
- [104] M.V. Galynskii, E.A. Kuraev, *JETP Letters*, **96**, 6 (2012).
- [105] M.V. Galynskii, E.A. Kuraev, *Phys.Rev.*, **D 89** 054005 (2014).
- [106] O.V. Selyugin, *Ukr.J. of Physics*, v.41, (1996).
- [107] O.V. Selyugin, *PEPAN Letters.*, v. 20, (2023) 409. *Physics of Elementary Particles and Atomic Nuclei* v 93, (2023) 137.
- [108] C. Mena, L. F. Palhares, arxiv: 1804.09564.